Journal of Geochemical Exploration 124 (2013) 40–58

Contents lists available at SciVerse ScienceDirect

Journal of Geochemical Exploration

journal homepage: www.elsevier.com/locate/jgeoexp

Characterization of primary geochemical haloes for gold exploration at the Huanxiangwa gold deposit, China

Changming Wang [a,b,*], Emmanuel John M. Carranza [c], Shouting Zhang [a], Jing Zhang [a], Xiaoji Liu [d], Da Zhang [a], Xiang Sun [a], Cunji Duan [e]

[a] State Key Laboratory of Geological Processes and Mineral Resources, China University of Geosciences, Beijing 100083, China
[b] Shandong Gold Group Corporation Limited, Jinan 250100, China
[c] Faculty of Geo-Information Science and Earth Observation (ITC), University of Twente, Enschede, The Netherlands
[d] Laboratory of Environmental Geology, Graduate School of Engineering, Hokkaido University, Hokkaido 060 0808, Japan
[e] No.1 Geological Surveying Team, Henan Bureau of Geology and Mineral Exploration and Development, Luoyang, 473200, China

ARTICLE INFO

Article history:
Received 30 October 2011
Accepted 28 July 2012
Available online 3 August 2012

Keywords:
Primary geochemical halo
Element associations
Principal components analysis
Centered log-ratio transformation
Gold exploration
Huanxiangwa gold deposit

ABSTRACT

Recognition of primary geochemical haloes is one of the most important tools for exploring undiscovered mineral resources. This tool is being routinely applied in exploration programs at the Huanxiangwa gold deposit, Xiong'er Mountains, China. Sampling of unweathered rock for multi-element analysis has been undertaken in all completed and ongoing exploration and development work, including drilling and galleries. Samples have been analyzed for 12 elements (Au, Ag, Pb, Zn, Cu, Mo, As, Sb, Bi, Co, Ni and Ba) from unaltered andesites, altered andesites, altered rocks and mineralized altered rocks. To identify multi-element geochemical associations that can be used to recognize enrichment zones, the lithogeochemical datasets were subjected to centered log-ratio transformation to address the closure problem with compositional data, and the log-ratio transformed datasets were subjected to principal components analysis. Results of analyses show that, in the Huanxiangwa deposit, gold mineralization is characterized by a Au ± Ag ± Cu association, base-metal mineralization by a Zn–Pb–Ag–Cu ± As ± Sb ± Mo association, supra- and/or near-ore primary haloes in mineralized altered rocks by an As ± Sb ± Bi ± Ag ± Au ± Pb association, sub-ore primary haloes in altered andesites and altered rocks around gold mineralization by a Mo–Bi ± Sb ± Ba ± Zn ± Ag association, and the host andesites by a Ni–Co–Ba association. Analyses of axial and longitudinal primary haloes indicate that gold mineralization is overprinted base-metal mineralization in the western and deeper parts of the Huanxiangwa deposit. Modified enrichment indices for Au and linear Au productivity values also indicate extension of gold mineralization with base-metal overprint beneath the western parts of the deposit. Based on this, an exploration target zone extending ca. 200 m below the known ore body was delineated, in which the presence of gold mineralization has been successfully verified by drilling. This study concludes that characterization of primary geochemical haloes associated with known deposits, coupled with analysis of linear element productivities, facilitates vectoring toward ore. Characterization of primary haloes associated with known deposits using lithogeochemical data would benefit highly from applications of log-ratio transformations developed for compositional data analysis.

1. Introduction

Geochemistry is one of the most important tools for exploring for undiscovered mineral resources (Cameron et al., 2004; Carranza, 2008, 2011b; Carranza et al., 2009; Clarke and Govett, 1990; Gray et al., 1991; Hronsky, 2004; Hronsky and Groves, 2008; McCuaig et al., 2010; Wang et al., 2007, 2008). That is because hydrothermal mineral deposits, for example, are characterized by hypogene wallrock alterations and/or primary geochemical haloes (Eilu and Mikucki, 1998; Govett and Atherden, 1988; McCuaig and Kerrich, 1998; Pirajno and Bagas, 2008; Safronov, 1936). Since it was proposed in the 1930s, the concept of primary geochemical haloes has not fundamentally changed. However, over the years, various methods of mineral exploration have been developed based on that concept (cf. Beus and Grigorian, 1977; Deng et al., 2008, 2009a, 2011a; Filzmoser et al., 2009a, 2012; Gundobin, 1984; Hawkes and Webb, 1962; Levinson, 1974; Li et al., 1993, 1995, 1998; Rose et al., 1979; Safronov, 1936; Solovov, 1985; Wang et al., 2010c). In recent years, analysis of primary geochemical haloes has become more and more important as a reliable exploration tool for revealing the presence of

* Corresponding author at: China University of Geosciences, No.29, Xueyuan Road, Haidian District, Beijing, 100083, China. Tel.: +86 10 82322301; fax: +86 10 82321006.
E-mail address: wcm233@163.com (C. Wang).

0375-6742/$ – see front matter © 2012 Elsevier B.V. All rights reserved.
http://dx.doi.org/10.1016/j.gexplo.2012.07.011

hidden or non-outcropping deposits (Eilu and Groves, 2001; Goldberg et al., 2003; Li et al., 2006; Schmid and Taylor, 2009).

There are three basic types of zoning in primary geochemical haloes of mineral deposits—axial, longitudinal and transversal. Research into 3-dimensional variations of primary geochemical haloes in mineral deposits has focused mainly on axial zoning, which is linked to the flow direction of ore-bearing fluids (Beus and Grigorian, 1977; Chen and Liu, 2000; Li et al., 1995, 1998, 2006). In steeply dipping orebodies, axial zoning coincides with vertical zoning; in sub-horizontal ore bodies, axial zoning coincides with horizontal zoning (cf. Beus and Grigorian, 1977; Harraz, 1995). Longitudinal zoning follows the strike of mineralization, whereas transversal zoning is approximately orthogonal to the strike of mineralization (Beus and Grigorian, 1977; Chen and Liu, 2000; Ghavami-Riabi et al., 2008; Goldberg et al., 2003; Harraz, 1995; Huston, 2001; Large and McGoldrick, 1998; Li et al., 1995, 1998, 2006; MacKenzie et al., 2007).

Primary geochemical haloes are multi-component, in the context of geochemical indicator trace elements. Different types of deposits have their own indicator elements. For example, primary haloes of various gold deposits have been described by indicator elements such as Ba, Au, Sb, As, Ag, Pb, Zn, Mo, Cu, Bi, Co, Ni, W, I and Be (Boyle, 1974, 1979, 1984; Chen and Liu, 2000; Eilu and Groves, 2001; Eilu and Mikucki, 1998; Fedikow and Govett, 1985; Goldberg et al., 2003; Govett et al., 1984; Harraz, 1995; Li et al., 1995, 1998, 2006; Wang et al., 2007). Primary haloes of gold deposits may show axial zoning of indicator elements such as Au, As, Bi, Ag, Pb, Sb, Cu, Be, Ma, Co and Zn, or they may show transversal zoning of indicator elements such as Sb, As, Ag, Pb, Zn, Cu, Bi, Mo, Au, Co, Be (Govett et al., 1984; Gundobin, 1984; Harraz, 1995; Kitaev, 1991; Ovchinnikov and Grigorian, 1971; White, 1981).

Some Chinese geologists (e.g., Chen and Liu, 2000; Li et al., 1995, 1998, 2006; Wang et al., 2007) have reported that geochemical zoning of indicator elements in hydrothermal gold (vein) deposits in China may form overlapping supra-ore (Hg, As, Sb, (B, F, I, Ba)), near-ore (Au, Ag, Pb, Zn, Cu) and sub-ore (Bi, Mn, Co, Ni) haloes. Geochemical zoning can be recognized for individual orebodies and single-stage metallogenic processes (Fig. 1).

The main motivation of the present study is that relatively few studies have concentrated on the analysis of primary geochemical haloes as a tool for exploration of hidden hydrothermal gold deposits. In previous studies, including some of those cited above, analyses of primary geochemical haloes were based on few and mainly mobile elements. Multi-element lithogeochemical data in the Huanxiangwa gold deposit provide a good opportunity to investigate primary geochemical haloes in relation to hydrothermal gold mineralization. That is because the Huanxiangwa gold deposit is mainly hidden but its geological and structural settings are well-understood (Wang et al., 2006a, 2006b, 2006c, 2007), providing a basis for the interpretation of primary geochemical haloes. The work presented here aims, therefore, to characterize the primary geochemical haloes of the Huanxiangwa gold deposit and to demonstrate prognostication of exploration targets using multi-element lithogeochemical data.

2. The Huanxiangwa gold deposit

2.1. Regional geology

2.1.1. Geotectonic setting

The Huanxiangwa gold deposit is situated in the northeastern Xiong'er Terrane of Xiaoqinling–Xiong'er Mountains (Fig. 2). This mountain range at the southern margin of the Sinokorean (or North China) craton is a result of the complex tectonic evolution of central China related to the continental collision between the Sinokorean and the Yangtze Cratons during the Mesozoic (Chen and Wang, 2011; Chen et al., 2006; Deng et al., 2009b, 2010, 2011b, 2011c; Hu and Lin, 1988; Wang et al., 2010a, 2010b; Zhou and Lu, 2000). This collision finally produced the Qinling Orogen of central China (Fig. 2), which extends for more than 2000 km, separating the Sinokorean Craton from the Yangtze Craton. More than 100 gold deposits and occurrences are concentrated in the Xiaoqinling (west), Xiaoshan (middle) and Xiong'ershan (east) areas. Deposits in the Xiaoqinling (Dongchuang, Wenyu, Yangzhaiyu and Dahu) and Xiaoshan areas are best classified as orogenic gold deposits, with ores occurring in a number of distinct belts both in quartz veins and disseminated in altered metamorphic rocks (Mao et al., 2005). In the Xiong'er Mountains, some of the gold deposits represent more shallowly emplaced tellurium-enriched orogenic systems, such as Shanggong and Beiling (Chen et al., 2006; Mao et al., 2005). Others are epithermal

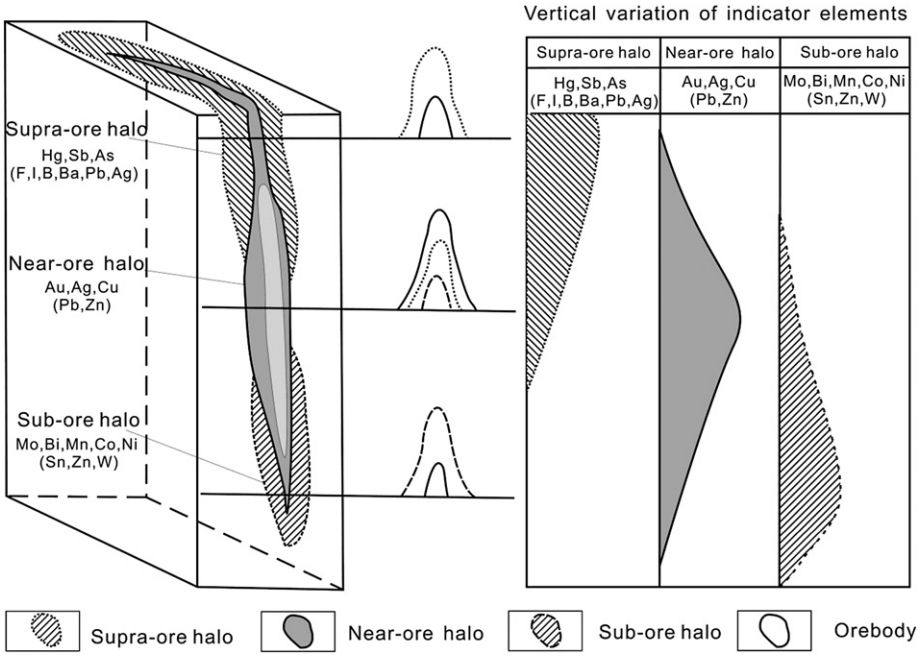

Fig. 1. Ideal element distribution pattern in primary haloes around gold deposits in China. Adapted from Li et al. (1995).

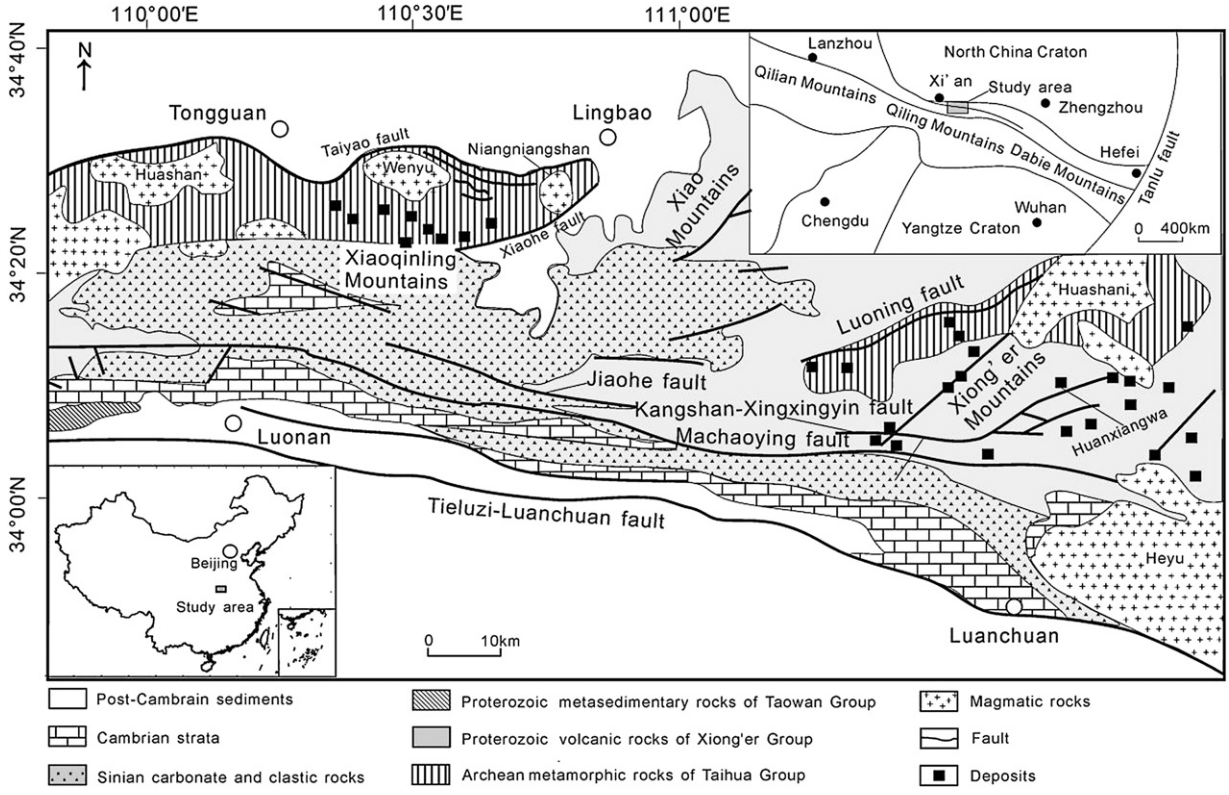

Fig. 2. Simplified regional geological map of the area where the Xiaoqinling and Xiong'er Mountains are situated, showing locations of major gold deposits including the Huanxiangwa gold deposit.
Adapted from No. 1 Geological Surveying Team (2003).

deposits (e.g., Qiyugou and Dianfang) that are hosted in volcanic breccia pipes (Chen et al., 2009; Mao et al., 2005).

2.1.2. Lithostratigraphy

The stratigraphic sequence in the Xiaoqinling–Xiong'er Mountains mainly comprises the crystalline basement of the Late Archean Taihua Group, metavolcanic rocks of the Middle Proterozoic Xiong'er Group cover (Fig. 2). The Taihua Group is divided, from bottom to top, into the Huanchiyu, Guanyitang, Lujiayu and Qiangmayu Formations. These formations are metamorphosed to amphibolite and granulite facies (Hacker et al., 1996). Rocks of the Taihua Group have U–Pb zircon ages of 2.8–2.6 Ga, with xenocrystic zircons as old as 2.9 Ga (Kroner et al., 1988). Rocks of the Xiong'er Group are well-exposed in the Xiong'er Mountains and the Xiao Mountains (Fig. 2). The Xiong'er Group is divided, from bottom to top, into the Dagushi, Xushan, Jidanping and Majiahe Formations. These formations comprise a suite of volcanic rocks consisting of andesite, dacite, rhyolite and minor basalt, trachyliparite, trachyte and quartz arkose. The age of the Xiong'er Group is constrained by dating (Sun et al., 1991), such as SHRIMP U–Pb ages of 1826 ± 32–1840 ± 14 Ma from rhyolites, in addition to ages ranging from 2089 ± 12 to 2511 ± 10 Ma for xenocrystic zircons, and an isochron age of 1635 ± 6 Ma for the rhyolites.

2.1.3. Structures

The main structures of the Xiaoqinling–Xiong'er Mountains are faults and folds running roughly E–W. The faults include the regional Tieluzi–Luanchuan fault, Machaoying fault and many smaller faults (Fig. 2). In the Xiaoqinling area, there are several large E–W-striking folds. They are, from south to north, the Laoyacha anticline, the Qishuping syncline and the Wulicun anticline. The Taiyao, Huanchiyu, Guanyintang and Xiaohe faults, distributed from north to south, are the main regional faults in the area. The veins occur where the ductile shear zones developed along, or near, the axes of the large folds. About 500 auriferous quartz veins have been identified along the Laoyacha and the Wulicun anticlines, but only a few small veins have been identified in the Qishuping syncline. In the Xiong'ershan and Xiaoshan areas, the structures are more complicated and folds are typically not well-mapped. The major fault systems in the region are the Luoning and the Kangshan–Xingxingyin faults (Fig. 2).

2.1.4. Magmatic rocks

Six pulses of granitoid magmatism have been recognized in the Qinling Orogen (Lu, 1999; Mao et al., 2005): Late Archean (2.9–2.5 Ga) tonalites–trondhjemites–granodiorites, Early Proterozoic (2.0–1.6 Ga), Late Proterozoic (1.1–0.8 Ga) and Early Paleozoic (600–420 Ma) subduction-, collision- and post-collision-related granites, and Mesozoic granites emplaced during 230–190 Ma and 170–80 Ma. Most mapped granitoids in the Xiaoqinling–Xiong'er Mountains are Mesozoic in age. The Huashan, Wenyu and Niangniangshan stocks in the Xiaoqinling area, and the Huashani and Heyu stocks in the Xiong'er Mountains are among the larger plutons (Fig. 2). In the former area, dates determined by K–Ar or Rb–Sr methods include 176.9–172.5 Ma for the Wenyu pluton (Hu and Lin, 1988), 178–102 Ma for the Niangniangshan pluton (Hu and Lin, 1988; Sima, 1997), and 166–80 Ma for the Huashan pluton (Sima, 1997; Yan, 1993). Less abundant Mesoproterozoic and Neoproterozoic granitoids are also recognized in the region. In the latter area, the Huashani pluton yielded K–Ar ages of 155.36 ± 3.53–81.17 ± 1.92 Ma (Wang et al., 2006a) and the Heyu pluton yielded a SHRIMP U–Pb age of 131.8 ± 0.7 Ma (Han et al., 2007).

2.2. Deposit geology

2.2.1. Lithology

Situated ca. 2 km NE of the Huanxiangwa gold deposit is the Mesozoic Huashani granite (Fig. 2), which is mainly a biotite adamellite. It is reddish–pinkish in color, porphyritic in texture and composed of

K-feldspar (30–40%), oligoclase (25–35%), quartz (20–30%), biotite (5%) and amphibole (8%). The main accessory minerals observed in the Huashani granite include titanite, apatite, zircon and magnetite. The Huashani granite formed from magma that was a mixture of mainly mantle melts and lower crust melts assimilated during lithospheric thinning (Wang et al., 2006a). Based on stable isotope, trace element and REE compositions, Wang et al. (2006a, 2006b, 2006c, 2007) proposed that the Huashani granite is both the heat and major metal source for the Huanxiangwa gold mineralization.

The Huanxiangwa gold deposit, which is located between the easternmost #10 exploration line and the westernmost #31 exploration line (Fig. 3), is hosted in the Proterozoic Xiong'er Group of volcanic rocks (Fig. 3). These rocks are primarily of the shoshonite series and secondarily of the high-K calc-alkaline series (Zhao et al., 1996). Specifically, the Huanxiangwa gold deposit is hosted in the Xushan Formation of the Xiong'er Group, which is composed of andesites, amygdaloidal andesites, andesitic porphyries with minor mugearites and tuffs. The deposit is localized along the NW-trending Huanxiangwa F985 fault zone, which is ca. 3 km long and 10–30 m wide. This fault zone dips ca. 29° toward N35°E. Along this fault zone, where the stress mechanism of its formation and evolution changed from compression to tension (Wang et al., 2006c), well-developed cataclastic andesites with minor mylonites exist.

2.2.2. Hydrothermal alteration

Hydrothermal alterations associated with the Huanxiangwa gold deposit include silicification, sericitization, pyritization, K-feldspar alteration, chloritization and carbonation (Wang et al., 2006b, 2006c). A large alteration halo around the Huanxiangwa gold deposit, which is well-developed along the Huanxiangwa F985 fault zone and measures ca. 4 km long and 20–100 m wide, has been explored to depths of 300 m within the mining area. The alteration halo can be divided into three zones based on type and intensity of alteration and distribution of altered rocks (Fig. 4), although mineralogical changes from one zone to the next are gradual and, thus, there are no clear boundaries between them (Wang et al., 2006b, 2006c).

The proximal alteration zone (mineralized altered rock), developed in the inner main fault zone, is characterized by strong pyrite alteration (ca. 5–8%), K-feldspar alteration (ca. 55–80%) and silicification (ca. 5%) (Wang et al., 2006b, 2006c). The alteration mineral assemblage in the proximal alteration zone is mainly pyrite–K-feldspar with minor sericite–K-feldspar and chlorite–quartz–K-feldspar. Surrounding the proximal alteration zone is the intermediate alteration zone (weakly-mineralized altered rock). This zone, which consists of strongly altered andesite, is characterized by silicification, K-feldspar alteration and carbonation and, in some cases, very weak metal mineralization. Outwards from the intermediate alteration zone is the distal

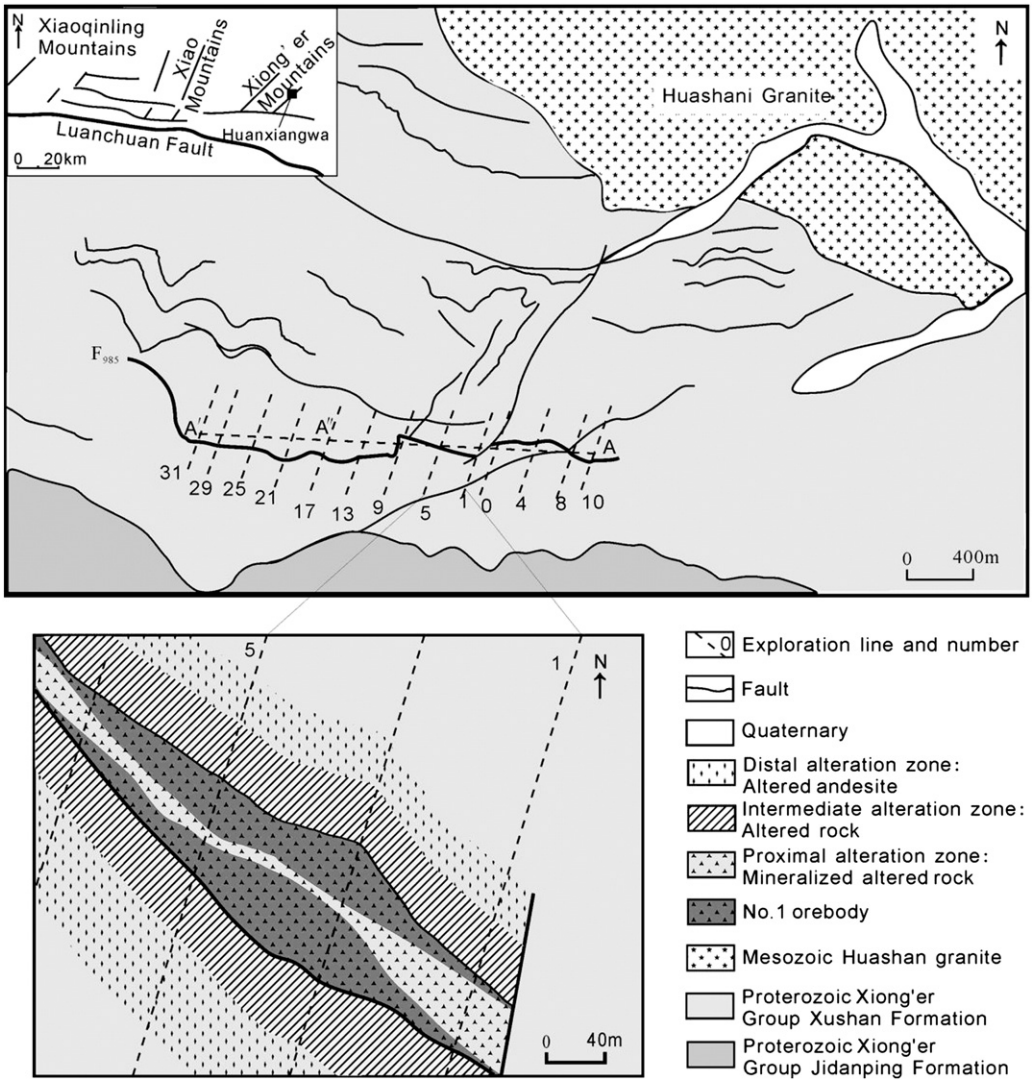

Fig. 3. Simplified geological maps of the Huanxiangwa district and the No. 1 orebody of the Huanxiangwa gold deposit (adapted from Wang et al., 2006b). Section A–A′ is shown in Fig. 10, whereas section A–A″ is shown in Fig. 12.

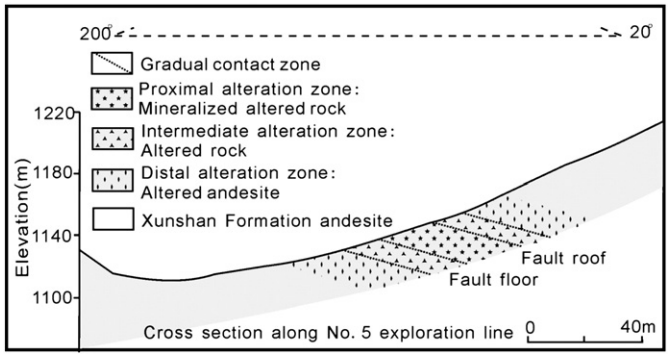

Fig. 4. Cross-section of the Huanxiangwa gold deposit along the #5 exploration line (after No. 1 Geological Surveying Team, 2003).

alteration zone (weakly altered andesite). This zone, which extends for as much as 40 m, is wider than either the proximal alteration or intermediate alteration zones (Fig. 4). Because it is farther away from the main fault zone, the intensity of alteration in the distal alteration zone is weaker than in the other two alteration zones (Wang et al., 2006b, 2006c).

2.2.3. No. 1 orebody

To date, about 10 orebodies have been found in the Huanxiangwa gold deposit. The No. 1 orebody, which is structurally-controlled by the Huanxiangwa F985 fault zone (Fig. 3), comprises more than 80% of the proven reserves of the Huanxiangwa gold deposit (Wang et al., 2006b, 2006c). It lies within the proximal alteration zone and extends vertically downwards to as much as 50 m parallel to the main fault zone (Fig. 3). It lacks sharp boundaries with other parts of the proximal alteration zone and it is distinguished mainly by a cut-off grade of 2 g/t Au (internal reports by the No. 1 Geological Surveying Team, Henan Bureau of Geology and Mineral Exploration and Development, Luoyang, China). Based on this cut-off grade, the length of the No. 1 orebody is 1300 m between the #10 and #17 exploration lines (Fig. 3), its average and maximum thickness are 5.29 m and 46.70 m, respectively, and its mean Au grade is 4.20 g/t. The orebody dips 29° toward N35°E. As observed in the open pit, the No. 1 orebody mainly comprises pyritized, sericitized and silicified andesite, with different degrees of cataclasis.

2.2.4. Ore mineralogy and paragenesis

Sulfide minerals in the Huanxiangwa gold deposit include mainly pyrite, sphalerite, galena, chalcopyrite and arsenopyrite. Pyrite is the most abundant and the main Au-bearing sulfide mineral in the deposit. Gold occurs dominantly in the lattices of sulfide minerals, and native gold occurs only in trace amounts. Gangue minerals dominantly comprise quartz, sericite, feldspar, calcite, barite and chlorite. Three stages of mineralization, from the earliest to the latest, have been identified: stage 1 of quartz–pyrite–K-feldspar; stage 2 of quartz–pyrite–gold; and stage 3 of quartz–base-metal sulfide minerals (Wang et al., 2006b, 2006c).

Stage 1 is defined by lenticular quartz veins/veinlets or pods with coarse-grained pyrite, K-feldspar and variable amounts of sericite in the associated alteration zones. The quartz is milk-white in color with a greasy luster, and is coarse-grained with subhedral habit. The pyrite is light yellow-white in color and has a strong metallic luster. It generally forms euhedral cubes with sides of 0.1–2.5 mm. The K-feldspar is allotriomorphic granular and measures 0.005–0.05 mm (Wang et al., 2006b, 2006c).

Stage 2 is the main gold mineralization period, during which large amounts of sulfide minerals, mostly pyrite, were precipitated. The pyrite is light yellow in color with a weak metallic luster. It generally forms euhedral and anhedral cubes and is fine- to medium-grained. The quartz is fine-grained and granular, with light gray color and a vitreous luster. Gold occurs mostly within the lattice of pyrite, or as the native mineral disseminated in trace amounts in quartz. This mineral assemblage forms veinlet and disseminated mineralization (Wang et al., 2006b, 2006c).

The mineral assemblage of stage 3 is composed dominantly of galena, chalcopyrite and pyrite, which form base-metal sulfide mineralization mainly within the hanging wall of the Huanxiangwa F985 fault zone. This stage is characterized by low-grade gold mineralization, which is uneconomic (Wang et al., 2006b, 2006c).

In addition to the above-discussed 3-stage mineralization paragenesis, there is a post-mineralization stage characterized by a mineral assemblage of mainly ankerite, calcite, quartz, barite and chlorite, occurring as veinlets in late fractures. In some cases, veins and veinlets of only ankerite or calcite occur.

2.2.5. Ore-forming fluids

One ankerite sample and three quartz samples from the Huanxiangwa gold deposit have been analyzed by Wang et al. (2006c) for fluid inclusions. The liquid components of fluid inclusions in the deposit consist mainly of K^+, Na^+ and Cl^-, with minor, Ca^{2+}, Mg^{2+} and F^-, and very little Li^+ and HCO^{3-} (Table 1) (Wang et al., 2006c). The K^+/Na^+, Ca^{2+}/Mg^{2+} and Cl^-/F^- ratios are variable, being 0.21–1.37 (average = 0.59), 0.79–2.23 (average = 1.36) and 13.00–43.48 (average = 28.52), respectively. The gaseous components of the fluid inclusions in the deposit are rich in H_2O (201.0–431.0 μg/g) with minor CO_2 (3.05–42.65 μg/g) (Table 1). The fluids associated with the deposit can be classified, therefore, as a NaCl–H_2O–CO_2 system (Wang et al., 2006c).

Fluid inclusion data from quartz samples in the Huanxiangwa and adjacent gold deposits (Fan et al., 1993; Wang et al., 2006a, 2006c) and from quartz samples in unaltered Huashani granite (Wang et al., 2006a) indicate intimate relationship between fluids associated with the Huanxiangwa gold deposit and fluids associated with the Huashani granite (Fig. 5). Average homogenization temperatures of fluid inclusions in quartz and ankerite are 212 °C and 145 °C, respectively (Wang et al., 2006c) (Table 2). Fluid inclusions in quartz exhibit two homogenization temperature peaks at 180 °C and 210 °C, whereas fluid inclusions in ankerite exhibit two homogenization temperature peaks at 130 °C and 160 °C (Wang et al., 2006c). The former two homogenization temperature peaks correspond roughly to the above-discussed three stages of mineralization identified within the Huanxiangwa gold deposit. Salinities measured in the fluid inclusions are 0.90–7.50 wt.% NaCl eq. (average = 4.16 wt.% NaCl eq.) (Table 2) (Wang et al., 2006c). The average salinity for fluid inclusions in quartz

Table 1
Compositions of fluid inclusions in selected samples from the Huanxiangwa gold deposit (from Wang et al., 2006c). Abbreviations: Qtz = quartz; Ank = ankerite; Py = pyrite; Au = gold; BMS = base-metal sulfides.

Sample no.	Mineral	Stage	Liquid compositions (ppm)								Gas compositions (ppm)				
			K^+	Na^+	Ca^{2+}	Mg^{2+}	Li^+	F^-	Cl^-	SO_4^{2-}	H_2O	CO_2	CO	CH_4	H_2
B3/976-CD11	Qtz	Stage 2: Qtz–Py–Au	2.96	9.52	2.28	0.99	0.04	0.33	14.40	2.50	397.0	12.5	0.05	0.05	0.11
B6/976-CD13	Qtz	Stage 2: Qtz–Py–Au	1.84	8.88	1.26	1.59	0.03	0.40	13.70	2.80	360.0	143.0	0.50	0.13	0.11
Z1/997-CD13	Qtz	Stage 3: Qtz–BMS	0.94	1.84	1.05	1.16	0.01	0.28	3.64	1.25	201.0	150.0	0.50	0.10	0.09
B1/976-CD11	Ank	Post-mineralization stage	3.28	2.40	6.30	4.36	0.01	0.25	5.80	5.00	431.0	255.0	2.60	1.50	0.12

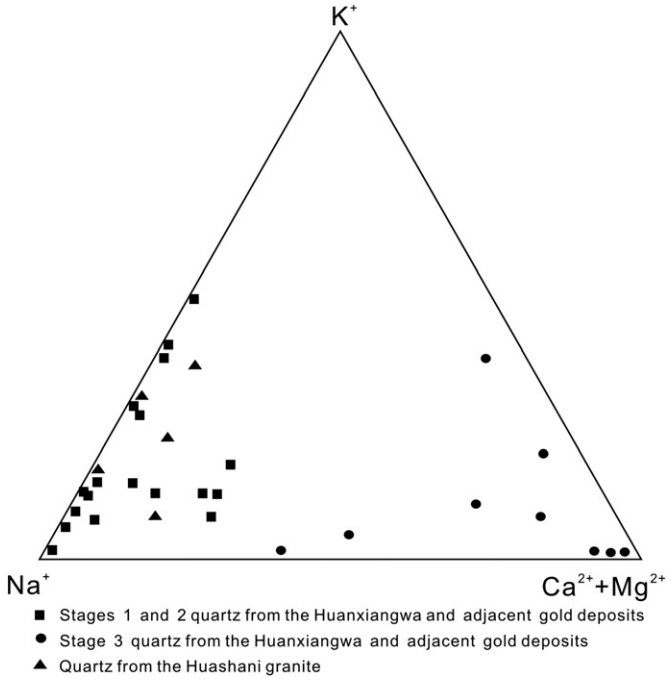

Fig. 5. Triangular diagram of Na^+–K^+–$Ca^{2+}Mg^{2+}$ composition of fluid inclusions in quartz samples from the Huashan granite and the Huanxiangwa gold deposit. Data are from Fan et al. (1993) and Wang et al. (2006a, 2006c).

and ankerite is, respectively, 5.38 and 0.55 wt.% NaCl eq. (Wang et al., 2006c).

3. Lithogeochemical data collection

3.1. Choice of trace elements

Earlier studies on primary haloes of more than 20 gold deposits in the Xiaoqinling–Xiong'er Mountains district (Li et al., 1993, 1995, 1998) revealed that primary haloes around orebodies are characterized by various indicator trace elements, such as Au, Ag, As, Sb, Ba, B, Hg, Cu, Pb, Zn, Bi, Mo, Mn, Co and Ni. For example, the Qinling, Wenyu and Dongtonggou gold deposits in that district have similar supra-ore (As–Sb), near-ore (Au–Ag–Pb–Zn–Cu) and sub-ore (Bi–Mo–Mn–Co–Ni) haloes, with vertical overlaps in their spatial distributions (Li et al., 1993, 1995, 1998). In the Xiaoqinling gold district, anomalous areas of Au–Ag–Cu–Pb–Zn–W element association occupy ca. 250 km^2; whereas in the Xiongershan gold district, anomalous areas of Au–Ag–Mo–Pb–Ba–Cu element association occupy ca. 500 km^2 (internal reports by the No. 1 Geological Surveying Team, Henan Bureau of Geology and Mineral Exploration and Development, Luoyang, China). Thus, based on those previous studies, twelve elements including (Au, Ag, Pb, Zn, Cu, Mo, Bi, Co, Ni, As, Sb and Ba) were considered for analysis of primary geochemical haloes in the Huanxiangwa gold deposit.

3.2. Sampling and chemical analysis

Sampling of unweathered rock was confined to nine exploration cross-sections and five levels (including the surface level and four underground levels) of the Huanxiangwa gold deposit. The rock samples (n = 389) collected include unaltered andesites (n = 104), altered andesites (n = 79), altered rocks (n = 83) and mineralized altered rocks (n = 123). The mineralized altered rocks are not based on cut-off grade but on the presence of visible sulfide minerals. Compared to altered andesites, the last two classes of rocks do not exhibit discernible characteristics of their protoliths. However, the Xushan Formation, which hosts the gold deposit, is chiefly andesite (Fig. 4). Thus, the protoliths of the altered rocks and mineralized altered rocks are likely andesites.

For the determination of Pb, Zn, Cu, Mo, Bi, Co, Ni and Ba by induced coupled plasma mass spectrometry (ICP-MS), ca. 100 mg of each sample was weighed into Teflon beakers and leached by 1.0 ml HF in an ultrasonic bath for several hours to dissolve silicates in the samples. The residues were then dissolved in 1.0 ml HF and 0.6 ml HNO_3 on a hotplate at ca. 190 °C overnight to digest sulfide and phosphate fractions. After that, the sample solutions were centrifuged, the supernatants were transferred to clean Teflon beakers, and the solutions were evaporated to near dryness. Then, 1.0 ml concentrated HNO_3 was added and dried twice to get rid of the HF or HCl in the samples. Finally, all samples were dissolved in 5 ml 5% HNO_3 solution spiked with an internal standard, Rh (10 ppb), prior to analysis.

For analysis of As and Sb by hydride generation-atomic fluorescence spectrometry (HG-AFS) using 2 ml KBH4 solution, 0.5 g of sample was dissolved in aqua regia and a mixed solution of 1% thiourea–ascorbic acid was added as a reductant. For analysis of Au and Ag by graphite furnace atomic absorption spectrophotometry (GF-AAS), ca. 10 g of sample was roasted at 650 °C for 2 h, and then decomposed in aqua regia. Then, 100 mg Fe^{3+} was added to the 100 ml solution in a 5% aqua regia medium. Gold and Ag in the solution were absorbed by polyurethane foam and desorbed with 1.2% thiourea solution.

The above-described analytical procedures were undertaken in the Chinese Academy of Geological Sciences. The analytical detection limits are 0.2 ppb for Au, 20 ppb for Ag, 0.05 ppm for Bi, 0.1 ppm for Sb and Co, 1 ppm for Cu, As, Ni and Ba, 2 ppm for Pb and Zn, and 0.2 ppm for Mo. The precisions (RSD %) of the analysis per element based on replicate measurements are 1.2% for Au, 3.4% for Ag, 4.5% for Pb, 4.4% for Zn, 3.5% for Cu, 2.3% for Mo, 1.4% for Bi, 2.2% for As, 1.5% for Sb, 1.6% for Co, 4.8% for Ni and 2.7% for Ba.

4. Lithogeochemical data analysis

Raw data of uni-element concentrations in the individual groups of rock samples are all strongly positively skewed (except Ba) (Table 3). Log10-transformation alleviates skewness in the data and shows that uni-element concentrations in the different classes of rock samples from the Huanxiangwa gold deposit are characterized by multiple populations (Fig. 6). The number of populations increases from unaltered andesites, to altered andesites, to altered rocks and to mineralized altered rocks. Concentrations of Mo, Ni and Ba seem to be described mainly by single populations in all classes of rock samples.

Table 2
Physico-chemical properties of fluid inclusions in selected samples from the Huanxiangwa gold deposit (from Wang et al., 2006c). Abbreviations: Qtz = quartz; Ank = ankerite; Py = pyrite; Au = gold; BMS = base-metal sulfides.

Sample no.	Mineral	Stage	Depth (km)	Homogenization temperature range (°C)	Homogenization temperature peak (°C)	Pressure ($\times 10^5$ Pa)	Salinity (wt.% NaCl eq.)
B3/976-CD11	Qtz	Stage 2: Qtz–Py–Au	0.68–0.77	160–285	225–265	200–230	4.9–7.5
B5/976-CD11	Qtz	Stage 2: Qtz–Py–Au	0.68–0.83	160–295	180–210	200–250	4.2–5.8
Z1/997-CD13	Qtz	Stage 3: Qtz–BMS	0.30–0.68	160–230	180–210	150–200	4.2–5.7
B1/976-CD11	Ank	Post-mineralization stage	1.01–1.31	117–204	130–160	305–395	0.9–2.0

Table 3
Statistical summary of trace element data (in ppm) of rock specimens from the Huanxiangwa gold deposit. Q1 = 1st quartile. Q3 = 3rd quartile. MAD = median of absolute deviation from data median. *EF* = enrichment factor (Eq. (1)).

	Au	Ag	Pb	Zn	Cu	As	Sb	Bi	Mo	Co	Ni	Ba
Mineralized altered rocks (n = 123)												
Minimum	0.01	0.06	0.3	1.2	1.52	0.01	0.14	0.01	0.20	4.12	0.45	122
5th %le	0.04	0.08	5.8	6.9	1.52	0.04	0.14	0.01	0.49	8.24	4.47	256
25th %le (Q1)	0.39	0.38	12.6	17.2	2.64	0.96	0.21	0.04	1.01	10.30	5.96	494
50th %le (Median)	1.53	1.01	29.2	46.4	8.09	2.35	0.43	0.11	1.68	12.83	7.83	725
75th %le (Q3)	2.10	2.37	111.6	107.2	16.50	5.78	0.72	0.21	2.65	24.38	16.74	921
95th %le	7.20	7.13	867.8	808.3	63.80	13.83	1.75	0.65	5.58	44.26	41.31	1256
Maximum	18.75	24.93	2152.7	6064.9	865.14	26.88	24.11	1.19	18.58	178.33	62.32	1453
MAD	1.00	0.80	21.4	32.0	6.08	1.80	0.29	0.07	0.70	3.65	2.49	196
Mean	2.15	2.10	155.0	202.7	23.77	4.67	1.00	0.18	2.35	20.44	13.45	720.1
Std. deviation	2.90	3.33	354.1	636.1	84.27	5.23	2.97	0.22	2.37	19.52	11.58	289.2
Skewness	3.31	3.98	4.0	7.3	8.66	2.02	6.90	2.31	3.67	4.84	1.92	0.2
EF	353.00	13.05	3.2	1.4	1.15	4.54	2.59	4.17	4.74	1.99	1.03	0.9
Altered rocks (n = 83)												
Minimum	0.01	0.04	1.2	13.0	2.84	0.09	0.48	0.07	0.78	7.27	2.76	281
5th %le	0.01	0.04	2.3	15.1	2.84	0.09	0.48	0.07	0.95	7.27	2.76	451
25th %le (Q1)	0.09	0.06	4.6	19.7	2.84	0.12	0.48	0.07	0.95	8.24	4.06	661
50th %le (Median)	0.18	0.16	9.2	24.2	6.19	0.41	0.48	0.07	1.03	9.21	4.79	871
75th %le (Q3)	0.37	0.57	26.1	64.3	25.69	1.32	0.49	0.17	1.23	12.61	6.64	1188
95th %le	1.01	2.32	622.1	586.9	46.69	3.34	1.61	0.70	3.82	18.91	14.38	1713
Maximum	1.02	5.09	959.5	2354.0	390.42	5.28	4.61	1.32	19.75	52.37	58.80	2470
MAD	0.17	0.11	6.5	6.9	3.35	0.32	0.00	0.00	0.08	1.45	1.11	231
Mean	0.29	0.52	87.6	141.2	19.13	0.93	0.70	0.19	1.54	11.79	6.82	960.1
Std. deviation	0.30	0.87	221.3	383.3	44.38	1.18	0.65	0.24	2.56	7.63	7.39	428.9
Skewness	1.25	3.01	3.3	4.3	7.34	1.82	4.46	2.63	6.91	4.11	5.30	1.1
EF	52.00	1.90	1.0	0.5	0.73	0.80	1.23	1.17	1.83	1.20	0.56	1.1
Altered andesites(n = 79)												
Minimum	0.01	0.08	6.9	43.1	8.98	0.18	0.34	0.12	0.74	9.58	6.81	87
5th %le	0.01	0.08	11.1	52.6	8.98	0.18	0.34	0.12	0.92	9.58	6.81	343
25th %le (Q1)	0.01	0.08	16.9	64.7	8.98	0.18	0.34	0.12	1.13	10.22	8.62	558
50th %le (Median)	0.01	0.08	26.2	78.5	8.98	0.18	0.34	0.12	1.13	11.49	9.98	757
75th %le (Q3)	0.01	0.12	50.4	91.9	8.98	0.46	0.34	0.12	1.19	13.41	11.80	919
95th %le	0.03	0.53	177.7	288.2	54.57	1.50	0.71	0.23	2.39	40.87	21.33	1412
Maximum	0.10	3.55	747.5	1509.9	131.89	10.14	1.18	1.10	6.59	56.19	37.67	2059
MAD	0.00	0.00	11.0	13.4	0.00	0.00	0.00	0.00	0.02	1.28	1.81	747.0
Mean	0.01	0.20	57.1	119.0	15.21	0.53	0.38	0.14	1.32	14.21	11.32	782.5
Std. deviation	0.01	0.48	113.2	185.8	19.49	1.20	0.14	0.13	0.85	9.43	5.23	336.2
Skewness	5.21	5.81	4.2	6.2	4.48	6.96	4.50	6.40	5.41	3.59	3.32	0.8
EF	1.0	0.40	2.1	1.4	0.51	0.14	0.87	2.00	1.80	1.39	1.09	1.9
Unaltered andesites (n = 104)												
Minimum	0.01	0.05	2.1	16.3	6.71	0.15	0.39	0.06	0.16	4.89	4.56	263
5th %le	0.01	0.05	4.3	22.7	6.71	0.15	0.39	0.06	0.30	4.89	5.17	466
25th %le (Q1)	0.01	0.05	6.8	31.1	6.71	0.20	0.39	0.06	0.39	6.19	6.38	709
50th %le (Median)	0.01	0.10	11.0	45.5	10.33	0.57	0.39	0.06	0.43	6.85	8.21	863
75th %le (Q3)	0.01	0.15	28.5	79.2	19.59	0.85	0.49	0.06	0.96	17.28	10.33	1051
95th %le	0.01	0.79	153.3	321.2	80.24	1.92	1.30	0.15	3.09	47.60	18.24	1509
Maximum	0.02	1.63	1205.5	3579.9	131.90	2.58	6.72	0.69	13.68	169.19	31.91	2073
MAD	0.00	0.05	5.8	15.9	3.62	0.37	0.00	0.00	0.11	1.63	2.12	171.5
Mean	0.01	0.18	51.6	121.9	21.17	0.71	0.58	0.08	1.01	15.41	9.25	906.3
Std. deviation	0.00	0.26	164.5	370.5	24.76	0.59	0.68	0.08	1.66	21.57	4.43	331.9
Skewness	−2.36	3.51	5.5	8.3	2.32	1.18	7.50	6.26	5.37	4.53	2.37	0.96
EF	1.00	1.00	1.00	1.00	1.00	1.00	1.00	1.00	1.00	1.00	1.00	1.00

4.1. Trace element enrichment and depletion

From unaltered andesites, to altered andesites, to altered rocks and to mineralized altered rocks, the median concentrations of Au, Ag, As and Mo show a general tendency of enrichment whereas the median concentrations of the other elements (Cu, Pb, Zn, Sb, Bi, Co, Ni and Ba) do not show distinct tendency of enrichment or depletion (Fig. 7). To determine trace element enrichment or depletion, a reference value for each element is required. A regional threshold for each element would be useful, but the regional element threshold values determined by the No. 1 Geological Surveying Team (2003) were obtained using the traditional method of data mean plus two standard deviations. Because of the problems with this method, as discussed by Reimann and Filzmoser (2000) and Reimann and Garrett (2005), we estimated local thresholds for the unaltered andesites (Table 3) equal to the data median plus two times the median absolute deviation (MAD) for each element (Reimann et al., 2005). Then, we defined enrichment factor (*EF*) as:

$$EF = [\text{median} + 2\text{MAD}]_{\text{rock sample group}} \div [\text{median} + 2\text{MAD}]_{\text{unaltered andesites}}. \quad (1)$$

Comparisons of the elemental data for altered andesites, altered rocks and mineralized altered rocks with those of unaltered andesites reveal the following (Table 3). Altered andesites are depleted in As, Ag, Cu and Sb but enriched in Pb, Zn, Bi, Mo, Co and Ba. Altered rocks are depleted in Zn, Cu, As and Ni but enriched in Au, Ag, Sb, Bi and Mo. Mineralized altered rocks are enriched in all elements except Ba.

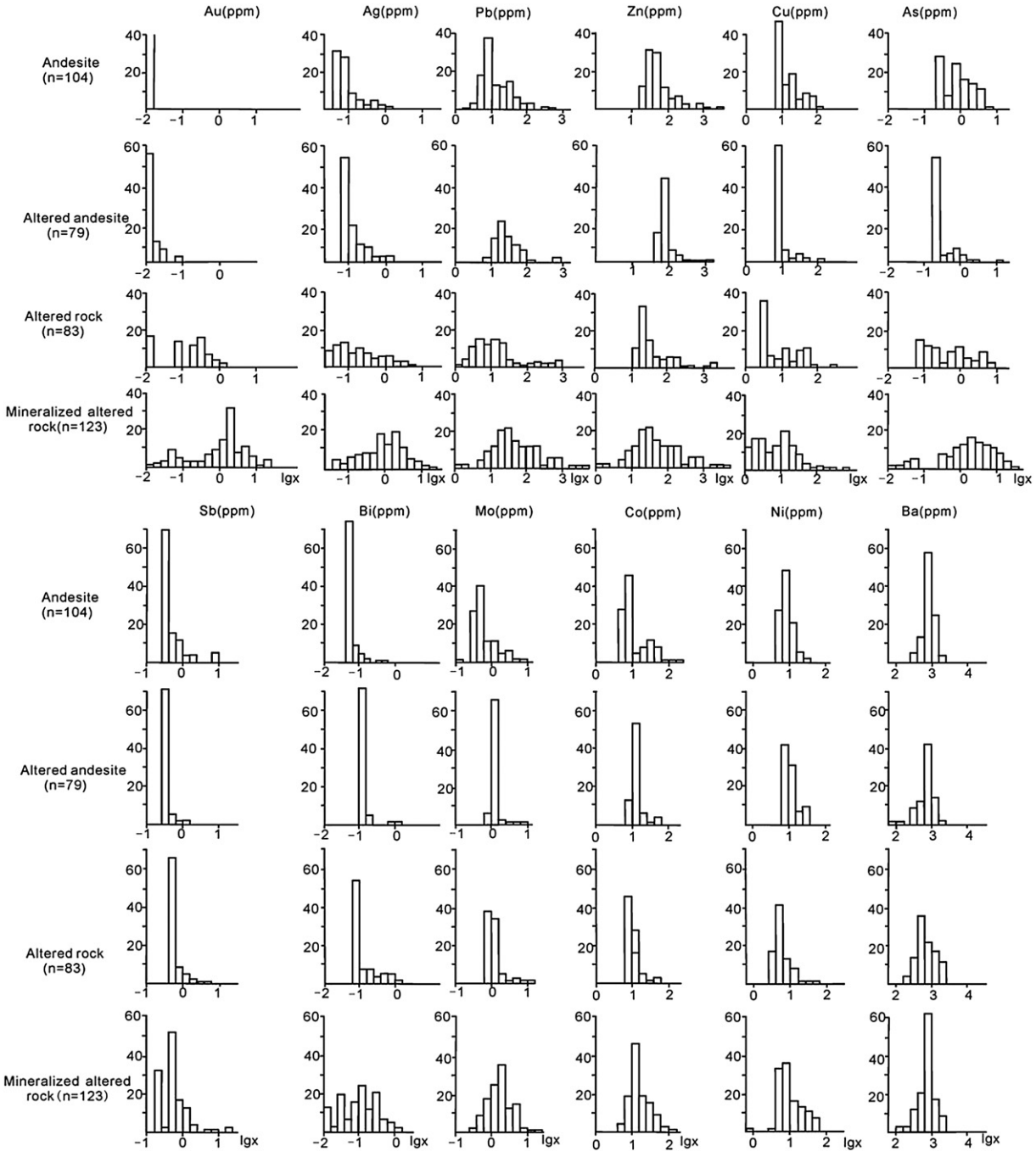

Fig. 6. Histograms of trace element contents (ppm; transformed to base 10 logarithms) in various rock specimens from the Huanxiangwa gold deposit.

Mineralized altered rocks are especially enriched in Au, Ag, As, Mo, Bi, Pb and Sb. These suggest that Au, Ag and As form haloes in Au-mineralized altered rocks whereas Mo, Bi and Sb form haloes in altered rocks around gold mineralization.

4.2. Trace element associations

To unravel the multi-element associations describing the different classes of rocks in the Huanxiangwa gold deposit, we performed principal components (PC) analysis (Howarth and Sinding-Larsen, 1983). To address the closure problem in multivariate statistical analysis of compositional datasets, we applied a centered log-ratio (CLR) transformation (Aitchison, 1986) to the elemental data prior to PC analysis (Carranza, 2011a; Reimann et al., 2002, 2008). We applied the Kaiser (1960) criterion to extract only PCs with eigenvalues greater than 1, meaning only PCs that explain as much variability equivalent of least one original variable are considered important. The extracted PCs were subjected to orthogonal rotation by the Varimax method (Kaiser, 1960) to maximize the variability (i.e. to strongly differentiate) among all input variables and, thus, facilitate interpretation of the factor loadings. To determine which PC loading is significant, we used the 'broken-stick' method (for details, see Peres-Neto et al., 2003).

The samples of mineralized altered rocks are described by four PCs (Table 4). PC1 (ca. 25% of multivariate data variability) represents antipathetic associations of Ni–Co–Ba(–Sb–Mo) and Ag–Pb(–Au), which reflect, respectively: (a) altered rocks around gold mineralization; and (b) base-metal sulfides associated with gold mineralization.

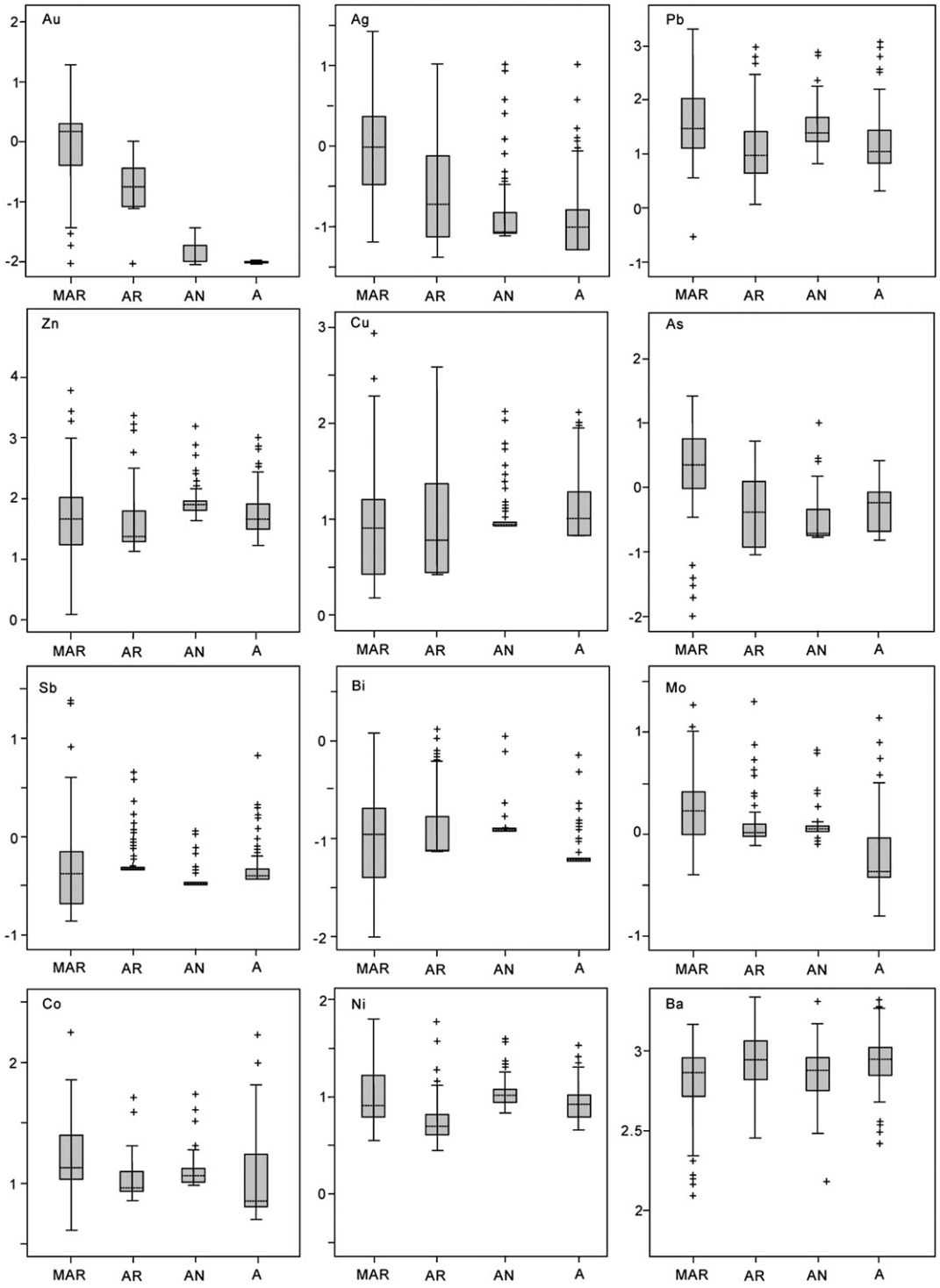

Fig. 7. Tukey boxplots of trace element contents (ppm; transformed to base 10 logarithms) in various rock specimens from the Huanxiangwa gold deposit. Abbreviations: MAR = mineralized altered rocks; AR = altered rocks; AN = altered andesites; A = unaltered andesites.

PC2 (ca. 17% of multivariate data variability) represents antipathetic associations of Bi–Mo(–Sb) and Zn–Cu(–Ag), which reflect, respectively: (a) geochemical haloes around Au-mineralized rocks; and (b) base-metal sulfide mineralization. PC3 (ca. 11% of multivariate data variability) represents antipathetic associations of Pb–Zn and Au (–Ag), which reflect, respectively: (a) base-metal sulfide mineralization; and (b) gold mineralization. PC4 (ca. 10% of multivariate data variability) represents antipathetic associations of Mo(–Ba–Zn) and As–Sb, which reflect, respectively: (a) geochemical haloes around Au-mineralized rocks; and (b) geochemical haloes in Au-mineralized rocks. The PC1–PC2 biplot (Fig. 8, upper left) portrays the multi-element associations representing the major processes associated with mineralized altered rocks in the Huanxiangwa deposit, namely: (i) Ni–Co–Ba–Sb–Mo, describing rocks (likely andesites) affected by hydrothermal alteration; (ii) Zn–Cu, describing base-metal sulfide mineralization; and (iii) Ag–Pb–Au–As, describing gold mineralization with base-metal sulfides.

The samples of altered rocks are described by four PCs (Table 4). PC1 (ca. 38% of multivariate data variability) represents antipathetic associations of Mo–Sb–Ba–Co (–Ni) and Pb–Ag–As, which reflect,

Table 4
Results of PC analyses of four datasets of rock geochemical data from the Huanxiangwa gold deposit. Values in bold are significant loadings determined using the broken-stick method (Peres-Neto et al., 2003).

Mineralized altered rocks ($n=123$)					Altered rocks ($n=83$)				
	PC1	PC2	PC3	PC4		PC1	PC2	PC3	PC4
Au	−0.304	0.038	**−0.857**	−0.018	Au	0.120	−0.388	**−0.732**	0.153
Ag	**−0.653**	−0.210	−0.286	0.083	Ag	**−0.674**	**−0.482**	0.082	0.339
Pb	**−0.604**	−0.065	**0.616**	0.003	Pb	**−0.715**	−0.289	**0.427**	−0.097
Zn	−0.126	**−0.651**	**0.459**	0.282	Zn	−0.019	**−0.456**	**0.547**	**−0.554**
Cu	−0.157	**−0.592**	0.120	0.175	Cu	−0.097	−0.049	**−0.797**	−0.254
As	−0.173	0.196	0.000	**−0.820**	As	**−0.602**	−0.196	0.187	−0.053
Sb	0.409	0.237	−0.086	**−0.525**	Sb	**0.724**	0.122	0.153	−0.241
Bi	−0.251	**0.676**	0.191	−0.043	Bi	−0.070	−0.122	0.129	**0.928**
Mo	0.252	**0.558**	0.001	**0.507**	Mo	**0.763**	0.165	0.323	0.124
Co	**0.761**	−0.124	−0.131	0.156	Co	**0.417**	**0.797**	0.082	0.004
Ni	**0.798**	0.001	0.124	−0.125	Ni	0.198	**0.910**	0.208	−0.028
Ba	**0.680**	0.112	0.007	0.360	Ba	**0.554**	**0.699**	0.000	−0.075
Eigenvalues	3.042	2.053	1.353	1.182	Eigenvalues	4.624	1.943	1.458	1.035
% of variance	25.351	17.106	11.277	9.854	% of variance	38.530	16.194	12.148	8.623
Cum. % of variance	25.531	42.457	53.733	63.587	Cum. % of variance	38.530	54.724	66.872	75.495
Altered andesites ($n=79$)					Andesites ($n=104$)				
	PC1	PC2	PC3	PC4		PC1	PC2	PC3	PC4
Au	0.137	−0.045	−0.052	**0.940**	Au	**0.868**	0.281	0.179	0.131
Ag	**−0.826**	−0.032	0.276	−0.185	Ag	−0.370	**−0.786**	−0.064	0.249
Pb	**−0.724**	−0.405	0.036	−0.216	Pb	−0.340	−0.378	**−0.643**	0.173
Zn	**−0.508**	0.064	**−0.646**	0.211	Zn	−0.132	−0.099	**−0.808**	−0.067
Cu	0.160	0.035	**−0.489**	0.102	Cu	−0.038	−0.118	0.020	**−0.869**
As	0.182	**−0.798**	−0.237	−0.275	As	**−0.750**	−0.097	0.333	−0.048
Sb	**0.827**	−0.088	0.139	−0.120	Sb	**0.545**	−0.080	0.202	−0.324
Bi	−0.122	0.174	**0.888**	0.038	Bi	**0.590**	−0.313	0.253	**0.446**
Mo	**0.583**	0.225	**0.472**	0.070	Mo	−0.098	−0.099	**0.849**	−0.031
Co	0.141	0.181	−0.195	0.047	Co	−0.195	**0.776**	−0.251	0.260
Ni	0.324	**0.683**	−0.028	−0.364	Ni	0.073	**0.758**	**0.449**	0.225
Ba	0.147	**0.812**	0.023	−0.118	Ba	**0.515**	**0.491**	0.314	−0.015
Eigenvalues	3.266	2.018	1.629	1.097	Eigenvalues	3.719	1.919	1.750	1.264
% of variance	27.217	16.818	13.575	9.145	% of variance	30.992	15.992	14.587	10.531
Cum. % of variance	27.217	44.035	57.610	76.755	Cum. % of variance	30.992	46.984	61.571	72.102

respectively: (a) altered rocks associated with gold mineralization; and (b) base-metal sulfide mineralization. PC2 (ca. 16% of multivariate data variability) represents antipathetic associations of Ni–Co–Ba (–Mo) and Ag–Zn (–Au–Pb), which reflect, respectively: (a) altered rocks around gold mineralization; and (b) base-metal sulfides associated with gold mineralization. PC3 (ca. 12% of multivariate data variability) represents antipathetic associations of Zn–Pb (–Mo–Ni) and Cu–Au, which reflect, respectively: (a) base-metal sulfide mineralization; and (b) gold mineralization. PC4 (ca. 8% of multivariate data variability) represents antipathetic associations of Bi (–Ag–Au) and Zn (–Cu–Sb), which reflect, respectively: (a) geochemical haloes in Au-mineralized rocks; and (b) base-metal sulfide mineralization. The PC1–PC2 biplot (Fig. 8, upper right) portrays the multi-element associations representing the major processes associated with altered rocks in the Huanxiangwa deposit, namely: (i) Ni–Co–Ba–Mo–Sb, describing rocks (likely andesites) affected by hydrothermal alteration; (ii) Pb–Ag–As describing base-metal sulfide mineralization; and (iii) Zn–Au–Bi describing gold mineralization with base-metal sulfides.

The samples of altered andesites are described by four PCs (Table 4). PC1 (ca. 27% of multivariate data variability) represents antipathetic associations of Sb–Mo (–Ni–As) and Ag–Pb–Zn, which reflect, respectively: (a) altered andesites associated with gold mineralization; and (b) base-metal sulfide mineralization. PC2 (ca. 17% of multivariate data variability) represents antipathetic associations of Ba–Ni (–Mo–Co) and As (–Pb), which reflect, respectively: (a) altered andesites around gold mineralization; and (b) geochemical haloes in Au-mineralized rocks. PC3 (ca. 14% of multivariate data variability) represents antipathetic associations of Bi–Mo (–Ag) and Zn–Cu (–As), which reflect, respectively: (a) geochemical haloes around Au-mineralized rocks; and (b) base-metal sulfides associated with mineralization. PC4 (ca. 9% of multivariate data variability) represents a Au(–Zn) association reflecting gold mineralization and associated base-metal sulfides. The PC1–PC2 biplot (Fig. 8, lower left) portrays the multi-element associations representing the major processes associated with altered andesites in the Huanxiangwa deposit, namely; (i) Ba–Ni–Mo–Sb, describing andesites affected by hydrothermal alteration; (ii) Ag–Pb–Zn describing base-metal sulfide mineralization; and (iii) As–Au–Cu describing gold mineralization with base-metal sulfides.

The samples of unaltered andesites are described by four PCs (Table 4). PC1 (ca. 31% of multivariate data variability) represents antipathetic associations of Au–Bi–Sb–Ba and As(–Ag–Pb), which reflect, respectively: (a) enrichment of gold and associated elements; and (b) base-metal enrichment independent of gold enrichment. PC2 (ca. 17% of multivariate data variability) represents antipathetic associations of Co–Ni–Ba (–Au) and Ag (–Pb–Bi), which reflect, respectively: (a) unaltered andesites with gold enrichment; and (b) base-metal enrichment independent of gold enrichment. PC3 (ca. 15% of multivariate data variability) represents antipathetic associations of Mo–Ni (–As–Ba–Sb–Au) and Zn–Cu (–Co), which reflect, respectively: (a) unaltered andesites with gold enrichment and associated elements; and (b) base-metal enrichment independent of gold enrichment. PC4 (ca. 11% of multivariate data variability) represents antipathetic associations of Bi (–Co–Ag–Ni) and Cu (–Sb), which reflect, respectively: (a) unaltered andesites; and (b) base-metal enrichment independent of gold enrichment. The PC1–PC2 biplot (Fig. 8, lower right) portrays the multi-element associations representing

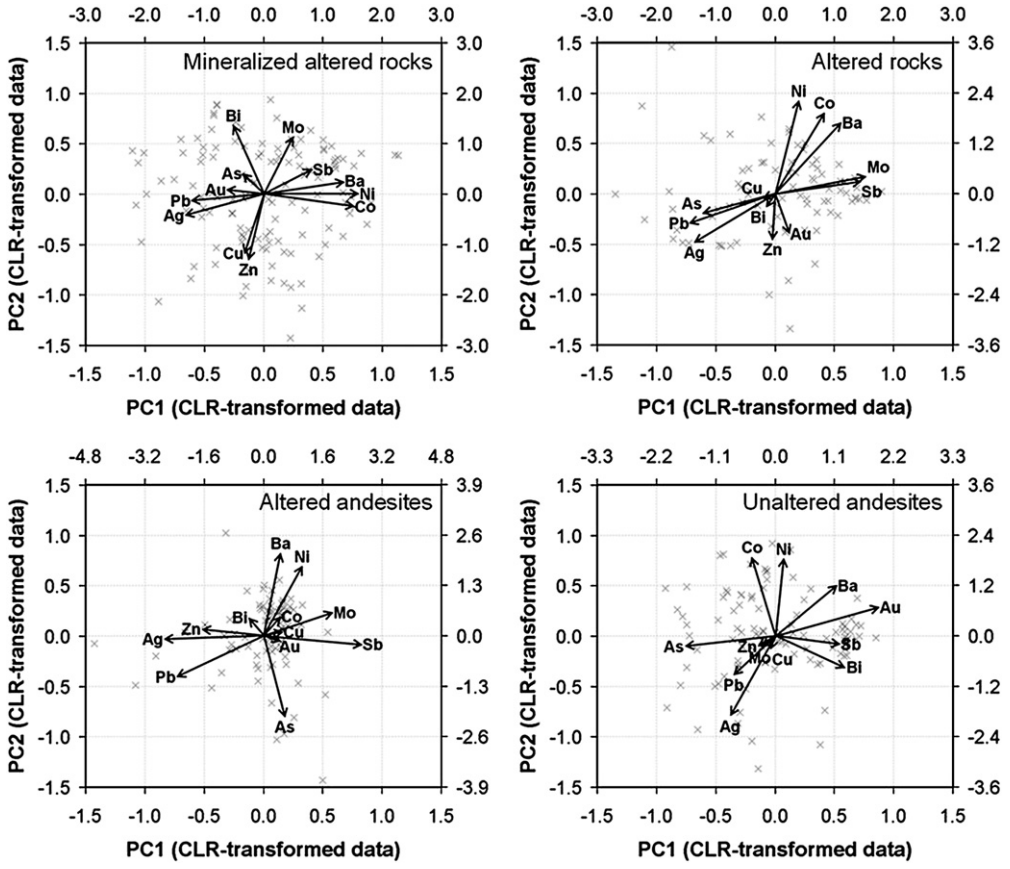

Fig. 8. Biplots of varimax rotated principal components analysis of trace element data for four classes of rock specimens from the Huanxiangwa gold deposit.

the major processes associated with unaltered andesites in the Huanxiangwa deposit, namely: (i) Co–Ni–Ba, describing andesites unaffected by hydrothermal mineralization; (ii) Ag–As–Pb, describing base-metal enrichment; and (iii) Au–Sb–Bi, describing gold enrichment.

Therefore, the four trace element datasets for the different classes of rocks in the Huanxiangwa deposit describe mainly seven geochemical associations reflecting: (1) gold mineralization—Au ± Ag ± Cu; (2) geochemical haloes around Au-mineralized rocks—Mo–Bi ± Sb ± Ba ± Zn ± Ag; (3) geochemical haloes in Au-mineralized rocks—As ± Sb ± Bi ± Ag ± Au ± Pb; (4) base-metal sulfides associated with gold mineralization—Ag–Zn ± Pb ± Au; (5) base-metal mineralization or enrichment independent of gold mineralization—Zn–Pb–Ag–Cu ± As ± Sb ± Mo; (6) altered rocks/andesites—Ba–Ni–Co ± Mo ± Sb; and (7) unaltered andesites—Ni–Co–Ba. In these associations, elements linked by a '–' occur commonly and thus form the principal elements of an association, whereas elements preceded a '±' occur less commonly and thus only form auxiliary elements of an association.

5. Analysis of primary haloes

5.1. Axial primary haloes

5.1.1. Uni-element variations with depth

To study the variations of each element with depth, we first determined the elemental enrichment factors (Eq. (1)) in the all underground levels (i.e. at elevations of 1100 m, 1023 m, 997 m and 976 m) in the Huanxiangwa deposit. Comparisons of elemental data from samples in the four underground levels with those from the samples unaltered andesites reveal the following (Table 5). Gold is strongly enriched (i.e. $EF \geq 10$) in all four levels, Cu is strongly depleted (i.e. $EF < 0.5$) in level 1023 whereas most of the other elements are weakly enriched (i.e. $1 < EF < 2$) and some elements are weakly depleted (i.e. $1 > EF > 0.5$). These results are, however, not instructive regarding primary geochemical haloes because values of *EF* do not take into account data variability. Accordingly, for example, the elements Ni, Co and Ba, which characterize the unaltered andesites, are indicated by the *EF* to be only weakly enriched or weakly depleted (Table 5); however, one would expect these elements to be strongly depleted relative to enrichment of metals associated with mineralization. Therefore, we next studied the 'ore-forming' index (*YQ*), which is actually a modified *EF* (Chen and Liu, 2000) of every element in the four underground levels.

As proposed by Chen and Liu (2000), *YQ* is the product of *EF* and data standard deviation. However, according to Filzmoser et al. (2009b, p. 6100), the standard deviation (or the variance) makes no statistical sense with closed data (e.g., compositional data). In addition, Filzmoser et al. (2009b, p. 6106) stated that for the compositional data the coefficient of variation is not needed but instead the variance of isometric log-ratio (ILR) transformed data can be used. Therefore, we applied ILR transformation (Egozcue et al., 2003) to the elemental data for samples in the four underground levels, and then we obtained the variance ('Var') of the ILR-transformed datasets. Then, we re-defined *YQ* as

$$YQ = EF' \mathrm{Var}_{\mathrm{ILR-transformed\ data}}. \quad (2)$$

Unlike the *EF* values, the *YQ* values of Ni, Co and Ba, which characterize the unaltered andesites, are mostly $0.4 < YQ < 0.6$ (Table 5). In contrast, the *YQ* values of many of the other elements are mainly $1 > YQ > 3$ with median *YQ* greater than 1. For Cu and Sb, *YQ* values are < 1 with medians of 0.87 and 1.03, respectively. For Au, *YQ* values are strongly variable but > 30. It can be interpreted that the elements with *YQ* values of mostly > 1 form three groups: (i) Au—representing gold mineralization; (ii) Ag, Pb, Zn—representing base-metal mineralization; and (iii) As, Bi,

Table 5
Enrichment factors (*EF*, Eq. (1)) and 'ore-forming' indices (*YQ*, Eq. (2)) derived from medians and measures of variability of trace element data (in ppm) of rock specimens from four underground levels in the Huanxiangwa gold deposit. MAD = median of absolute deviation. Var = variance. ILR = isometric log-ratio.

	Au	Ag	Pb	Zn	Cu	As	Sb	Bi	Mo	Co	Ni	Ba
1100 m level (n = 54)												
Median	0.49	0.41	35.1	65.0	8.98	1.45	0.38	0.12	1.47	11.55	9.31	745
MAD	0.48	0.33	23.7	26.2	3.26	1.27	0.05	0.01	0.34	1.25	2.04	97
$Var_{ILR\text{-}transformed\ data}$	4.28	1.19	0.9	1.1	0.98	1.34	0.33	0.62	0.38	0.37	0.51	0.83
EF	145.00	5.33	3.6	1.5	0.88	3.04	1.23	2.33	3.31	1.39	1.08	0.78
YQ	620.73	6.35	6.2	1.6	0.86	4.07	0.40	1.44	1.26	0.52	0.55	0.64
1023 m level (n = 35)												
Median	0.04	0.22	17.7	34.6	3.85	0.80	0.48	0.07	1.06	10.26	7.83	895
MAD	0.03	0.16	10.0	16.3	1.10	0.58	0.05	0.03	0.32	2.02	3.36	130
$Var_{ILR\text{-}transformed\ data}$	3.21	0.63	0.8	1.0	0.44	0.91	1.06	0.89	0.50	0.29	0.42	0.72
EF	10.00	2.70	1.7	0.9	0.34	1.50	1.49	2.17	2.62	1.41	1.17	0.96
YQ	32.06	1.70	1.4	0.8	0.15	1.35	1.57	1.93	1.31	0.41	0.49	0.69
997 m level (n = 64)												
Median	0.27	0.19	18.0	59.8	8.98	0.59	0.48	0.12	1.13	10.28	6.63	739
MAD	0.26	0.13	9.4	33.5	5.45	0.41	0.14	0.05	0.15	1.55	2.10	178
$Var_{ILR\text{-}transformed\ data}$	4.22	0.87	1.0	1.3	0.77	0.93	0.37	0.85	0.43	0.31	0.48	0.50
EF	79.00	2.25	1.6	1.6	1.13	1.08	1.95	3.67	2.20	1.32	0.87	0.91
YQ	333.28	1.96	1.7	2.2	0.88	1.00	0.72	3.12	0.96	0.42	0.41	0.46
976 m level (n = 71)												
Median	0.17	0.16	20.5	52.6	8.98	0.67	0.48	0.12	0.13	10.85	7.26	602
MAD	0.16	0.11	15.9	33.6	6.14	0.58	0.14	0.05	0.18	2.12	2.65	239
$Var_{ILR\text{-}transformed\ data}$	3.42	1.37	1.4	1.3	1.57	1.79	0.68	0.85	0.63	0.28	0.41	0.79
EF	49.00	1.90	2.3	1.5	1.21	1.40	1.95	3.67	2.29	1.49	1.01	0.90
YQ	167.45	2.61	3.3	2.0	1.89	2.49	1.33	3.11	1.44	0.41	0.42	0.71

Mo—representing geochemical haloes in or around Au-mineralized rocks. This interpretation is consistent with the preceding interpretations of the PC analyses of trace element geochemical data for the different classes of rocks in the Huanxiangwa gold deposit.

Analyses of the *YQ* values of Ag, Pb, Zn, As, Bi and Mo show that the *YQ* values of As generally increase with elevation whereas the *YQ* values of Ag, Pb and Bi generally decrease with elevation. The *YQ* values of Zn and Mo do not exhibit apparent co-variations with elevation. These observations suggest axial zoning of Ag, Pb, As and Bi and that, with respect to gold mineralization, As forms near-ore (or even supra-ore) haloes whereas Ag, Pb and Bi form sub-ore haloes. These interpretations are consistent with axial zoning of indicator elements in primary haloes of gold deposits described in the literature (e.g., Govett et al., 1984; Gundobin, 1984; Harraz, 1995; Kitaev, 1991; Ovchinnikov and Grigorian, 1971; White, 1981).

5.1.2. Variations in multi-element associations with depth

To study variations in multi-element associations with depth, we considered two depth intervals—'deep' and 'shallow'—in the Huanxiangwa deposit based on available data. Thus, we created two new datasets, with the least difference in number of samples, by combining data for mineralized altered rocks, altered rocks and altered andesites (a) from 976 m and 997 m levels of the Huanxiangwa deposit ($n = 150$ samples), and (b) from 1023 m and 1100 m levels of the Huanxiangwa deposit ($n = 135$ samples). The latter dataset forms the 'shallow' interval (>1000 m elevation), the former the 'deep' interval (<1000 m elevation). To unravel multi-element associations describing axial primary halo zoning, we applied the same procedures of data transformation and PC analysis described in Section 4.2.

The samples of mineralized altered rocks, altered rocks and altered andesites from the shallow (>1000 m elevation) parts of Huanxiangwa deposit are described by three PCs (Table 6). PC1 (ca. 40% of multivariate data variability) represents antipathetic associations of Ni–Co–Ba–Sb–Mo and Ag–Pb–Au–As, which reflect, respectively: (a) rocks (likely andesites) affected by hydrothermal alteration; and (b) base-metal sulfides associated with gold mineralization. PC2 (ca. 17% of multivariate data variability) represents antipathetic associations of Zn–Cu–Pb and Au–As–Ag, which reflect, respectively: (a) base-metal sulfide mineralization; and (b) gold mineralization. PC3 (ca. 10% of multivariate data variability) represents antipathetic associations of Bi–Mo and As–Au–Zn, which reflect, respectively: (a) geochemical haloes around Au-mineralized rocks; and (b) gold and base-metal mineralization. The PC1–PC2 biplot (Fig. 9, upper left) portrays the multi-element associations representing the major processes associated with mineralized altered rocks, altered rocks and altered andesites in the 'shallow' levels of the Huanxiangwa deposit, namely: (i) Ni–Co–Ba–Sb–Mo, describing rocks (likely andesites) affected by hydrothermal alteration; (ii) Zn–Cu–As–Pb, describing base-metal sulfide mineralization; and (iii) Au–Ag, describing gold mineralization.

The samples of mineralized altered rocks, altered rocks and altered andesites from the deep (<1000 m elevation) parts of Huanxiangwa deposit are described by four PCs (Table 6). PC1 (ca. 26% of multivariate data variability) represents antipathetic associations of Co–Ni–Ba–Mo and Ag(–Cu–As–Au), which reflect, respectively: (a) rocks (likely andesites) affected by hydrothermal alteration; and (b) base-metal sulfides associated with gold mineralization. PC2 (ca. 18% of multivariate data variability) represents antipathetic associations of Sb–Bi–Mo and Ag–Au, which reflect, respectively: (a) geochemical haloes around Au-mineralized rocks; and (b) gold mineralization. PC3 (ca. 13% of multivariate data variability) represents antipathetic associations of Pb–Zn and Au(–Ba–Sb), which reflect, respectively: (a) base-metal mineralization; and (b) gold mineralization. PC4 (ca. 12% of multivariate data variability) represents antipathetic associations of Cu–Zn(–Ba) and As(–Au), which reflect, respectively: (a) base-metal mineralization; and (b) geochemical haloes in Au-mineralized rocks. The PC1–PC2 biplot (Fig. 9, upper right) portrays the multi-element associations representing the major processes associated with mineralized altered rocks, altered rocks and altered andesites in the 'deep' levels of the Huanxiangwa deposit, namely: (i) Co–Ni–Ba–Mo, describing rocks (likely andesites) affected by hydrothermal alteration; (ii) Sb–Bi, describing geochemical haloes around Au-mineralized rocks; (iii) Ag–Au, describing gold mineralization; and (iv) Cu–As–Pb–Zn, describing base-metal mineralization.

The stronger loadings of Ag, Au and As on PC1 of the 'shallow' dataset compared to those on PC1 of the 'deep' dataset and the higher variability explained by the PC1 of the 'shallow' dataset (ca. 40%)

Table 6
Results of PC analyses of two datasets of rock geochemical data from shallow and deep levels of the Huanxiangwa gold deposit. Values in bold are significant loadings determined using the broken-stick method (Peres-Neto et al., 2003).

Mineralized altered rocks, altered rocks, and altered andesites from the shallow (1100–1023 m) levels ($n=135$)				Mineralized altered rocks, altered rocks, and altered andesites from the deep (997–976 m) levels ($n=150$)				
	PC1	PC2	PC3		PC1	PC2	PC3	PC4
Au	**−0.510**	**−0.663**	**−0.368**	Au	−0.253	**−0.560**	**−0.666**	−0.255
Ag	**−0.743**	**−0.441**	−0.114	Ag	**−0.445**	**−0.726**	0.057	−0.186
Pb	**−0.655**	**0.461**	0.157	Pb	−0.186	−0.109	**0.862**	−0.173
Zn	0.022	**0.812**	−0.290	Zn	0.088	−0.066	**0.720**	**0.454**
Cu	0.024	**0.711**	0.084	Cu	−0.278	0.075	0.097	**0.711**
As	**−0.455**	**−0.561**	**−0.438**	As	−0.268	−0.031	0.003	**−0.809**
Sb	**0.614**	−0.103	0.179	Sb	−0.163	**0.677**	−0.383	−0.035
Bi	0.000	0.090	**0.902**	Bi	−0.160	**0.608**	0.108	0.092
Mo	**0.421**	−0.220	**0.429**	Mo	0.367	**0.597**	−0.055	−0.109
Co	**0.844**	0.096	0.083	Co	**0.832**	−0.161	−0.121	0.197
Ni	**0.847**	0.214	0.014	Ni	**0.824**	0.211	0.118	−0.174
Ba	**0.795**	0.303	0.135	Ba	**0.449**	0.306	−0.485	0.423
Eigenvalues	4.840	2.046	1.233	Eigenvalues	3.113	2.217	1.562	1.440
% of variance	40.334	17.050	10.273	% of variance	25.938	18.479	13.018	11.998
Cum. % of variance	40.334	57.384	67.656	Cum. % of variance	25.938	44.417	57.435	69.433

compared to that by the PC1 of the 'deep' dataset (ca. 26%) suggest that the main axial parts of the Huanxiangwa gold deposit occur mostly in the shallower levels (i.e. above 1000 m). The quite similar proportions of variability explained by the base-metal mineralization components of the 'shallow' dataset (PC2, ca. 17%) and the 'deep' dataset (PC3, 13%) suggest that base-metal sulfides are roughly uniformly distributed (or disseminated) within the deposit. The presence of both gold and base-metal mineralization components in the two datasets is consistent with the ore mineralogy and paragenesis of the deposit (see Section 2.2.4). The 'shallow' dataset reveals the presence of As-dominated geochemical halo components (PC1–PC3) in Au-mineralized rocks, whereas the 'deep' dataset reveals the presence of a Sb–Bi geochemical halo component (PC2) around Au-mineralized rocks. These results suggest that, in conjunction with the paragenesis of the deposit, the overprint of the base-metal mineralization on the gold mineralization occurs mainly in the deeper levels (i.e. below 1000 m) of the Huanxiangwa gold deposit. Moreover, the results suggest that, with respect to gold mineralization,

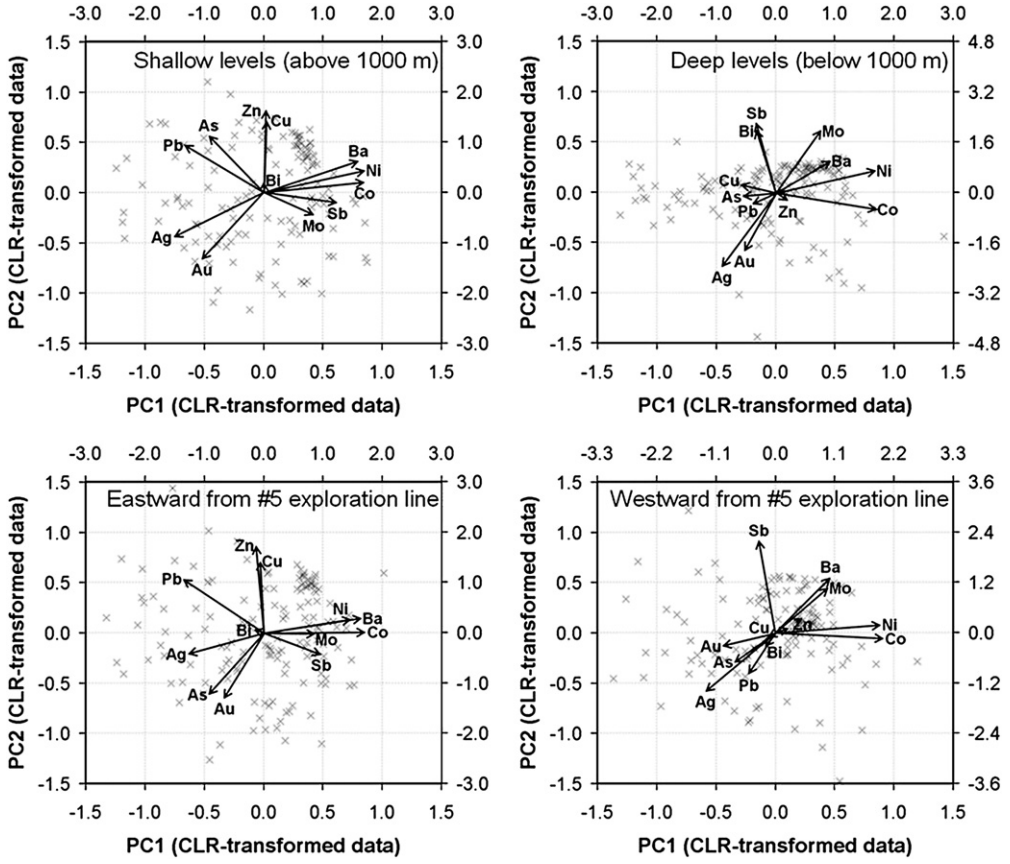

Fig. 9. Biplots of varimax rotated principal components of trace element data for three classes of rock specimens (mineralized altered rocks, altered rocks and altered andesites) from different parts of the Huanxiangwa gold deposit.

As forms near-ore (or even supra-ore) haloes whereas Sb and Bi form sub-ore haloes. These latter interpretations are consistent with the preceding interpretations of the *YQ* values.

5.2. Longitudinal primary haloes

To unravel the element associations describing the primary halo longitudinal zoning, we created two new datasets—'eastern' and 'western'—by combining data for mineralized altered rocks, altered rocks and altered andesites: (a) from the #5 exploration line to the eastern parts of the Huanxiangwa gold deposit ($n = 138$ samples); and (b) from the #5 exploration line to the western parts of the Huanxiangwa gold deposit ($n = 147$ samples). The only reason for choosing the #5 exploration line as reference is to obtain two new datasets with the least difference in number of samples. Then, we applied the same procedures of data transformation and PC analysis described in Section 4.2.

The samples of mineralized altered rocks, altered rocks and altered andesites from the eastern parts of Huanxiangwa deposit are described by three PCs (Table 7). PC1 (ca. 33% of multivariate data variability) represents antipathetic associations of Co–Ba–Ni–Sb(–Mo) and Pb-Ag–As(–Au), which reflect, respectively: (a) rocks (likely andesites) affected by hydrothermal alteration; and (b) base-metal sulfides associated with gold mineralization. PC2 (ca. 19% of multivariate data variability) represents antipathetic associations of Zn–Cu–Pb and Au–As(–Sb–Ag), which reflect, respectively: (a) base-metal mineralization; and (b) gold mineralization and associated geochemical haloes. PC3 (ca. 11% of multivariate data variability) represents antipathetic associations of Bi–Sb(–Mo) and Au–Ag, which reflect, respectively: (a) geochemical haloes around Au-mineralized rocks; and (b) gold mineralization. The PC1–PC2 biplot (Fig. 9, lower left) portrays the multi-element associations representing the major processes associated with mineralized altered rocks, altered rocks and altered andesites in the eastern parts of the Huanxiangwa deposit, namely: (i) Co–Ba–Ni–Sb–Mo, describing rocks (likely andesites) affected by hydrothermal alteration; (ii) Zn–Cu–Pb, describing base-metal sulfide mineralization; and (iii) Au–As–Ag, describing gold mineralization.

The samples of mineralized altered rocks, altered rocks and altered andesites from the western parts of Huanxiangwa deposit are described by five PCs (Table 7). PC1 (ca. 32% of multivariate data variability) represents antipathetic associations of Co–Ni–Ba–Mo and Ag–Au(–As–Pb), which reflect, respectively: (a) rocks (likely andesites) affected by hydrothermal alteration; and (b) base-metal sulfides associated with gold mineralization. PC2 (ca. 17% of multivariate data variability) represents antipathetic associations of Sb–Ba–Mo and Ag–Pb(–As), which reflect, respectively: (a) geochemical haloes around Au-mineralized rocks; and (b) base-metal sulfides associated with gold mineralization. PC3 (ca. 11% of multivariate data variability) represents antipathetic associations of Zn–Pb and Au(–Ag–Mo), which reflect, respectively: (a) base-metal mineralization; and (b) gold mineralization. PC4 (ca. 10% of multivariate data variability) represents antipathetic associations of Bi–Ba(–Mo) and As(–Au), which reflect, respectively: (a) geochemical haloes around Au-mineralized rocks; and (b) geochemical haloes in Au-mineralized rocks. PC5 (ca. 9% of multivariate data variability) represents antipathetic associations of As(–Mo–Pb–Ag) and Cu(–Ba–Zn), which reflect, respectively: (a) geochemical haloes in Au-mineralized rocks; and (b) base-metal mineralization. The PC1–PC2 biplot (Fig. 9, lower right) portrays the multi-element associations representing the major processes associated with mineralized altered rocks, altered rocks and altered andesites in the 'western' parts of the Huanxiangwa deposit, namely: (i) Co–Ni–Ba–Mo, describing rocks (likely andesites) affected by hydrothermal alteration; (ii) Sb(–Ba–Mo), describing geochemical haloes around Au-mineralized rocks; (iii) Au–As, describing gold mineralization; and (iv) Ag–Pb, describing base-metal mineralization.

The similar proportions of variability explained by the altered rock component (PC1—ca. 33%) in the 'eastern' dataset and by the altered rock component (PC1—ca. 32%) in the 'western' dataset suggest a uniform degree of hydrothermal alteration within the Huanxiangwa gold deposit. In addition, the similar proportions of variability explained by the base-metal mineralization component (PC2—ca. 19%) in the 'eastern' dataset and by the base-metal mineralization components (PC2 and PC5—ca. 20%) in the 'western' dataset suggest that base-metal sulfides are quite uniformly distributed (or disseminated) within the Huanxiangwa gold deposit. However, the higher proportion of variability explained by the gold mineralization components (PC2, PC3—ca. 30%) in the 'eastern' dataset compared to that explained by the gold mineralization component (PC3—ca. 11%) in the 'western' dataset suggests the main longitudinal parts of the Huanxiangwa gold deposit occurs mostly east of the #5 exploration line. This interpretation is consistent with large-scale mapping of the No. 1 orebody (Fig. 3), which is wider to the east than to the west of the #5 exploration line.

The 'eastern' dataset reveals the presence of As-dominated geochemical halo components (PC1 and PC2) in Au-mineralized rocks, whereas the 'western' dataset reveals the presence of Sb–Bi geochemical halo components (PC2–PC4) around Au-mineralized rocks. These results suggest that, in conjunction with the paragenesis of the deposit, the overprint of the base-metal mineralization on the gold mineralization occurs mainly in the western parts of the Huanxiangwa gold deposit. Moreover, the results suggest that, with respect to gold

Table 7
Results of PC analyses of two datasets of rock geochemical data from western and eastern parts the Huanxiangwa gold deposit using #5 exploration line as reference (Fig. 3). Values in bold are significant loadings determined using the broken-stick method (Peres-Neto et al., 2003).

Mineralized altered rocks, altered rocks, and altered andesites westward from #5 exploration line ($n = 147$)				Mineralized altered rocks, altered rocks, and altered andesites eastward from #5 exploration lines ($n = 138$)					
	PC1	PC2	PC3		PC1	PC2	PC3	PC4	PC5
Au	−0.326	**−0.644**	**−0.544**	Au	**−0.431**	−0.135	**−0.755**	−0.244	0.109
Ag	**−0.628**	−0.212	**−0.458**	Ag	**−0.578**	**−0.580**	−0.268	−0.171	0.218
Pb	**−0.663**	**0.515**	0.116	Pb	−0.218	**−0.402**	**0.705**	−0.022	0.294
Zn	−0.059	**0.853**	0.196	Zn	0.105	0.037	**0.811**	−0.016	−0.202
Cu	−0.024	**0.688**	0.066	Cu	−0.012	−0.025	0.085	−0.013	**−0.921**
As	**−0.456**	**−0.610**	−0.030	As	−0.332	−0.288	−0.071	**−0.565**	**0.464**
Sb	**0.482**	−0.218	**0.539**	Sb	−0.136	**0.896**	−0.045	−0.187	0.071
Bi	−0.050	0.021	**0.871**	Bi	−0.072	−0.136	0.083	**0.898**	0.086
Mo	0.432	−0.008	0.279	Mo	**0.435**	**0.435**	−0.205	0.286	0.323
Co	**0.856**	0.001	−0.103	Co	**0.902**	−0.059	0.033	0.084	−0.091
Ni	**0.729**	0.122	0.118	Ni	**0.877**	0.071	0.170	−0.089	0.072
Ba	**0.804**	0.142	0.182	Ba	**0.453**	**0.532**	−0.064	**0.403**	−0.257
Eigenvalues	3.972	2.310	1.332	Eigenvalues	3.810	2.031	1.350	1.211	1.042
% of variance	33.103	19.248	11.101	% of variance	31.750	16.927	11.246	10.093	8.680
Cum. % of variance	33.103	52.351	63.452	Cum. % of variance	31.750	48.677	59.924	70.017	78.697

mineralization, As forms near-ore (or even supra-ore) haloes whereas Sb and Bi form sub-ore haloes. These latter interpretations are consistent with the preceding interpretations of the *YQ* values.

To cross-validate the preceding interpretations of the PC analyses of the 'eastern' and 'western' datasets, we interpolated, by using an ordinary inverse-distance weighting technique, the elemental data points at or near the vertical plane represented by line A′–A that is almost parallel to the Huanxiangwa F_{985} fault zone and, thus, longitudinal to the Huanxiangwa deposit (Fig. 3). Then, we classified the interpolated elemental data using intervals listed in Table 8, which have been defined by the No. 1 Geological Surveying Team (1993, 2003) for identifying geochemical anomalies based on regional elemental threshold values. The classified interpolated elemental data on the vertical plane A′–A show that the main longitudinal parts of the gold mineralization occur mostly east of the #5 exploration line as depicted by the distributions of Au, As and Sb (Fig. 10). In contrast, the main longitudinal parts of the base-metal mineralization occur mostly west of the #5 exploration line, depicted by the distributions of Bi, Ag, Pb, Cu and Zn. In addition, the classified interpolated uni-element data on the vertical plane A′–A show that the main axial parts of the gold mineralization occur mostly above the 997 m level and that the distributions of Sb, Mo, Cu and Zn describe a sub-ore halo to gold mineralization in the Huanxiangwa gold deposit. Therefore, the multi-element associations derived from PC analyses (Tables 6 and 7), which represent axial and longitudinal primary geochemical haloes, are generally consistent with the elemental data distributions in the vertical profile A′–A (Fig. 10).

5.3. Transversal primary haloes

Because the orebody of the Huanxiangwa deposit dips 29°, on average, toward the NE, horizontal transversal zoning coincides roughly with axial zoning (cf. Beus and Grigorian, 1977; Harraz, 1995). Therefore, we opted to study transversal primary haloes along the #3 exploration line, which crosses the widest parts of the No. 1 orebody (Fig. 3). However, we did not perform PC analysis to unravel element associations describing the transversal primary haloes along the #3 exploration line because the samples-to-variables ratio was less than 3:1 (Arrindell and van der Ende, 1985). However, based on the results of analysis of multi-element associations in the lithogeochemical data (Section 4.2) and the results of analysis of axial primary haloes (Section 5.1), the data shown in Fig. 11 can be interpreted as follows. The As ± Sb ± Bi ± Ag ± Au ± Pb association characterizing the sides of the hanging wall and the Mo–Bi ± Sb ± Ba ± Zn ± Ag association characterizing the sides of the footwall represent geochemical haloes, respectively, in and around Au-mineralization near the wallrocks. These observations indicate that transversal primary haloes related to gold mineralization are concentrated along the sides of hanging wall and footwall of the Huanxiangwa F_{985} fault.

5.4. Exploration significance of primary haloes

Gold and Ag, as indicator elements of gold mineralization, are present in various element associations derived from the different subsets of the lithogeochemical data for analysis of primary haloes in the Huanxiangwa gold deposit. The distributions of the elemental data and the variations of multi-element associations with depth illustrate overprinting of gold and base-metal mineralizations in the deposit, with gold mineralization occurring mainly in the shallower parts of the deposit and base-metal mineralization occurring mainly in the deeper parts of the deposit. Because the overprint of the base-metal mineralization on the gold mineralization occurs mainly in the deeper levels of the Huanxiangwa gold deposit (see Section 5.1.2), it is plausible that gold mineralization still exists at greater depths. Therefore, we calculated linear Au productivity values for every sample along every exploration line and in every underground level. Then, we interpolated by an ordinary inverse-distance weighting technique the Au productivity data points at or near the vertical plane represented by line A″–A (Fig. 12).

In a plane (e.g., a cross-section), the linear productivity of an element in anomalous geochemical halo is the product of the average content (in percent) of an element defining the halo multiplied by the width of the halo (in meters), and its units are meter·percent (Ovchinnikov and Grigorian, 1971). The linear productivity (P_L) of an indicator element (e.g., Au) can be estimated as (Ovchinnikov and Grigorian, 1971):

$$P_L = (C_a - C_b)W \tag{3}$$

where C_a is average of anomalies (i.e. values greater than a threshold), C_b is average of background (i.e. values less than or equal to a threshold) and W is the width of anomalous halo (in meters) in a cross-section. In this paper, the widths of anomalous haloes were determined based on regional elemental threshold values in Table 8 (e.g., Au > 0.05 ppm).

Interpolated values of linear Au productivity tend to increase toward deeper levels in the western parts along cross-section A″–A (Fig. 12), suggesting that gold mineralization with base-metal overprint exists beneath the western parts of the present Huanxiangwa gold deposit. This interpretation is supported by results of the PC analyses of subsets of the lithogeochemical data for identifying axial primary haloes (Section 5.1.2) and longitudinal primary haloes (Section 5.2). The major multi-element associations in the western parts of the Huanxiangwa deposit (Fig. 9, upper right) are strongly similar to those in the deeper levels of this deposit (Fig. 9, lower right), whereas the major multi-element association in the eastern parts of the deposit (Fig. 9, upper left) are strongly similar to those in the eastern parts of this deposit (Fig. 9, lower left). Therefore, analyses of primary geochemical haloes associated with known deposits coupled with analysis of linear element productivity provides for vectoring toward ore. Accordingly, the exploration target zone was extended ca. 200 m below the known ore body (i.e. between 900 and 700 m levels) (Fig. 12). At least four drillholes successfully verified the presence of gold mineralization in the exploration target zone. Based on those four drillholes, a new ore body was outlined with average grade of 3.05 g/t Au, average thickness of 5.29 m, and estimated Au resources and reserves of 5.52 Mt and 16.83 t, respectively.

6. Conclusions

Primary geochemical haloes in the Huanxiangwa gold deposit are associated with hydrothermally altered rocks, which extend 20–100 m

Table 8
Intervals of individual trace element data (in ppm) used to classify primary geochemical anomalies for identifying primary geochemical axial zoning in the Huanxiangwa gold deposit.

Zoning	Au	Ag	Pb	Zn	Mo	Cu	As	Sb	Bi	Co	Ni	Ba
Background	<0.05	<0.3	<100	<200	<2	<50	<0.8	<0.5	<0.1	<20	<20	<1000
Distal	0.05–2	0.3–1.2	100–200	200–400	2–4	50–100	0.8–1.5	0.5–1	0.1–0.2	20–40	20–40	1000–1500
Intermediate	2–5	1.2–3.0	200–400	400–800	4–8	100–400	1.5–3.0	1–4	0.2–0.3	40–80	40–80	1500–2000
Proximal	>5	>3.0	>400	>800	>8	>400	>3.0	>4	>0.3	>80	>80	>2000

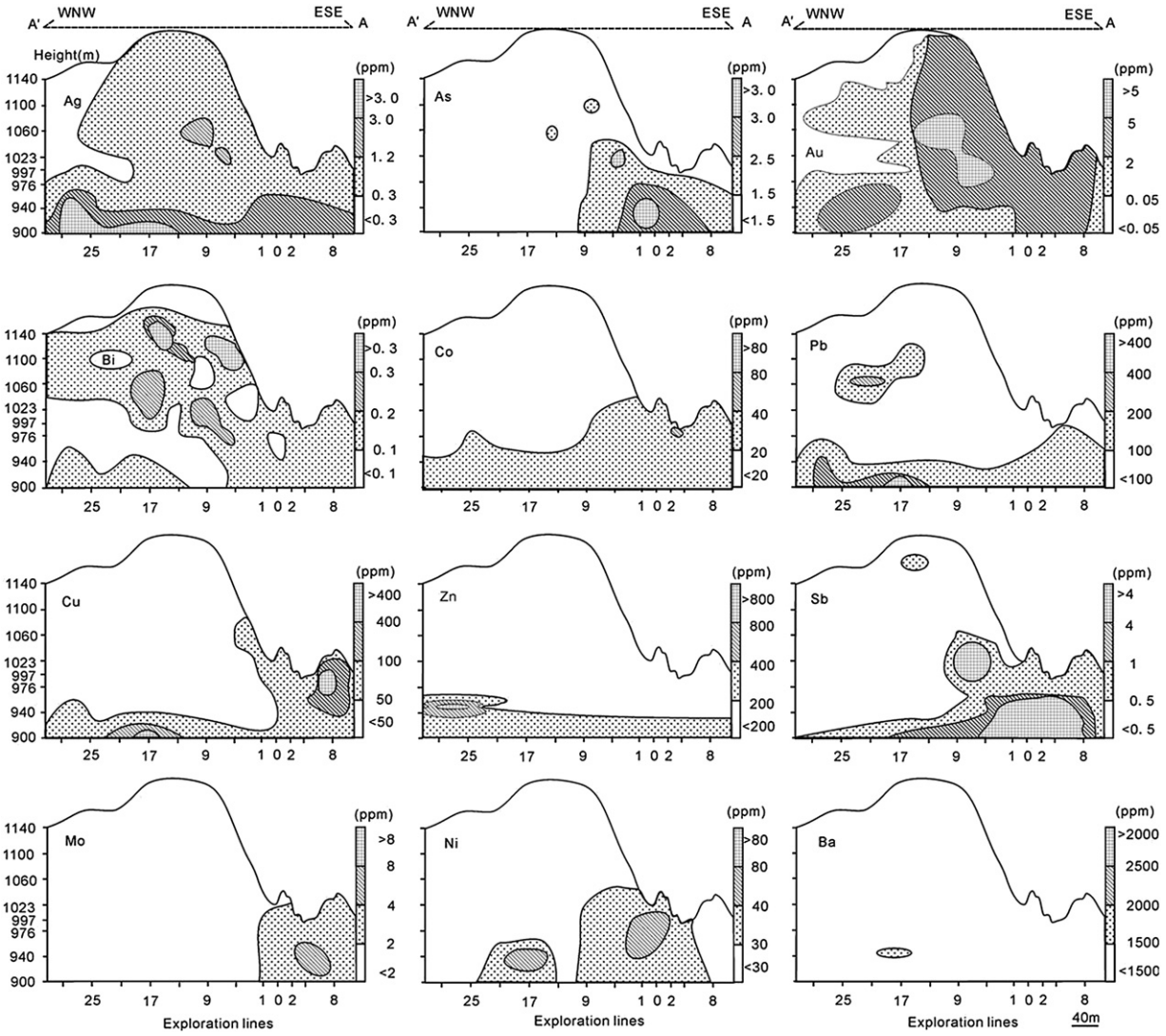

Fig. 10. Vertical profiles of trace element distributions describing primary axial and longitudinal geochemical zoning in the Huanxiangwa gold deposit.

across the strike of the major F_{985} fault zone. During the formation and evolution of this fault zone, the stress mechanism changed from compression to tension resulting in increased structural permeability of rocks that favored hydrothermal fluid-flow and eventually hydrothermal alteration of surrounding rocks and formation of the Huanxiangwa gold mineralization. Based on type and intensity of hydrothermal alteration and the distribution of altered rocks, three alteration zones can be distinguished (proximal, intermediate, distal) with respect to the fault zone, although there are no clear boundaries between them. The proximal alteration zone (mineralized altered rock) is characterized by strong pyrite alteration, K-feldspar alteration and silicification. The intermediate alteration zone (weakly-mineralized altered rock) is characterized by silicification, K-feldspar alteration, carbonation and, in some cases, very weak metal mineralization. The distal alteration zone (weakly altered andesite) is farther away from the fault zone, and its alteration intensity is weaker than those of the other two zones. The most intensely altered parts of the fault zone have abundant quartz veins, silicified breccias and silicified wallrocks, all of which contain base-metal sulfides and gold. Sulfide minerals in the deposit include pyrite, sphalerite, galena, chalcopyrite and arsenopyrite. Pyrite is the most abundant sulfide and the main Au-bearing mineral within the deposit.

Analysis of different subsets of the present lithogeochemical data reveals several multi-element associations describing the mineralizations and geochemical haloes present in the Huanxiangwa gold deposit. The main gold mineralization is generally described by a $Au \pm Ag \pm Cu$ association, whereas the late-stage base-metal mineralization is generally described by a $Zn–Pb–Ag–Cu \pm As \pm Sb \pm Mo$. Supra- and/or near-ore haloes in mineralized altered rocks are generally described by an $As \pm Sb \pm Bi \pm Ag \pm Au \pm Pb$ association, whereas sub-ore haloes in altered andesites and altered rocks around gold mineralization are generally described by a $Mo–Bi \pm Sb \pm Ba \pm Zn \pm Ag$. The andesites are generally described by a Ni–Co–Ba association. Analysis of variations in multi-element associations in the vertical and horizontal directions suggests that: (a) gold mineralization occurs mainly in the shallower and eastern parts of the Huanxiangwa deposit; (b) base-metal mineralization is roughly uniformly distributed in the deposit; and (c) base-metal mineralization overprints gold mineralization at depths. Calculated and interpolated values of linear gold productivity based on axial primary halo zoning indicate the existence of new gold resources at depth, which were confirmed by drilling.

Characterization of primary geochemical haloes associated with known deposits coupled with analysis of linear element productivity provides for vectoring toward ore. The characterization of primary geochemical haloes presented here benefitted from the applications of statistical procedures (i.e. using median and median of absolute deviation) for exploration data analysis rather than for confirmatory data analysis. Statistical parameters (e.g., mean and standard

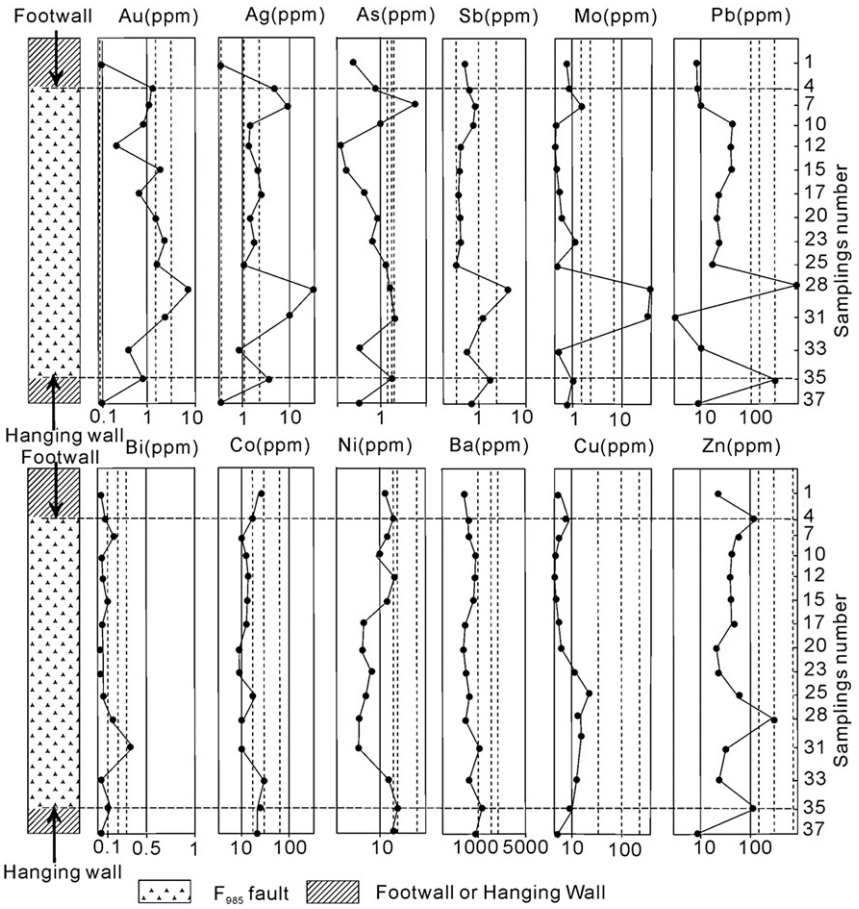

Fig. 11. Example of primary halo transversal zoning sequences from the #3 exploration line cross-section at 1023 m elevation of the Huanxiangwa gold deposit. The x-axes of the graphs represent trace element contents, whereas the y-axes represent sampling positions. Dashed lines represent the intervals of individual trace element data used for classifying primary geochemical anomalies listed in Table 8.

deviation) for confirmatory data analysis are suitable only for data with normal distributions, which is not the case for the present lithogeochemical data. The characterization of primary geochemical haloes presented here also benefitted from the applications of data transformations for compositional data analysis. The recognition and interpretation of important multi-element associations through principal components analysis were facilitated by the application of centered log-ratio transformation, but not by log-transformation, of

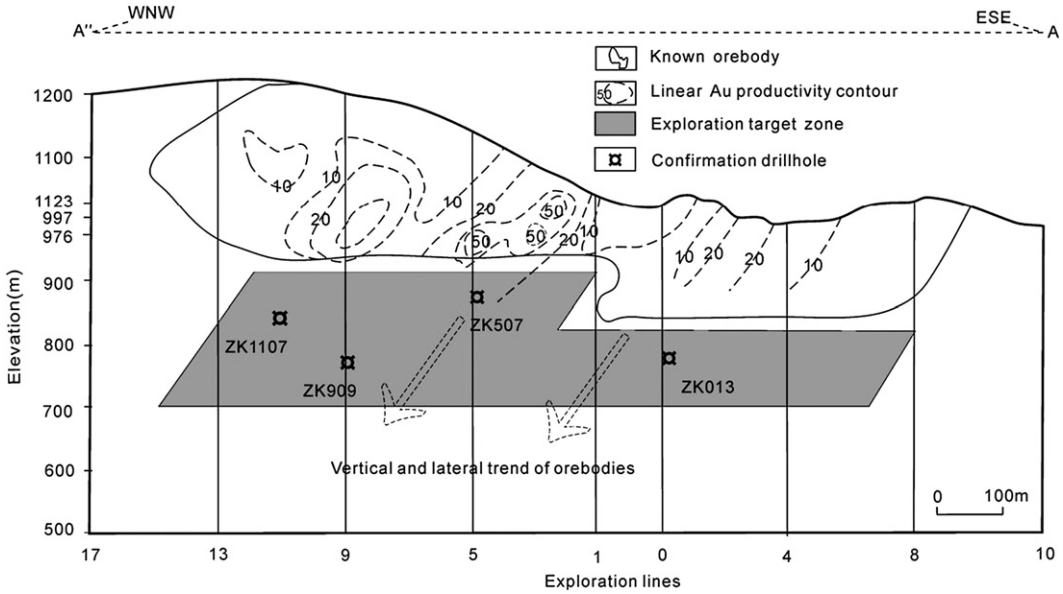

Fig. 12. Vertical profile showing distribution of linear Au productivity (P_L) values, based on which an exploration target zone was delineated beneath the known orebody of the Huanxiangwa gold deposit.

the data. Therefore, by applications of suitable statistical procedures for exploratory data analysis and suitable data transformations for compositional data analysis, the analysis of primary geochemical haloes linked with mineralization enhances its effectiveness as an exploration tool for revealing the presence (or absence) of the deposit type of interest at depths.

Acknowledgment

The authors acknowledge the National Basic Research Program (No. 2009CB421008), Fundamental Research Funds for the Central Universities (No. 2010ZY02), State Key Laboratory of Geological Processes and Mineral Resources (No. jointly supported this research GPMR201019), China Postdoctoral Science Foundation funded project (No. 20090460400), Program for Changjiang Scholars and Innovative Research Team in University (PCSIRT) and the 111 Project (No. B07011). We thank the anonymous reviewers for their critical reviews and constructive comments, which helped us improve significantly our paper.

References

Aitchison, J., 1986. The Statistical Analysis of Compositional Data. Chapman and Hall, London. 416 pp.
Arrindell, W.A., van der Ende, J., 1985. An empirical test of the utility of the observations-to-variables ratio in factor and components analysis. Applied Psychological Measurement 9, 165–178.
Beus, A.A., Grigorian, S.V., 1977. Geochemical Exploration Methods for Mineral Deposits. Applied Publishing, Wilmette. 287 pp.
Boyle, R.W., 1974. Elemental associations in mineral deposits and indicator elements of interest in geochemical line 39. prospecting: Geological Survey of Canada, paper, 74–45. 40 pp.
Boyle, R.W., 1979. The geochemistry of gold and its deposits. Geological Survey of Canada, Bulletin 280, 584p.
Boyle, R.W., 1984. The prospect for geochemical exploration—predictable advances and new approaches. Journal of Geochemical Exploration 21, 1–18.
Cameron, E.M., Hamilton, S.M., Leybourne, M.I., Hall, G.E.M., McClenaghan, M.B., 2004. Finding deeply buried deposits using geochemistry. Geochemistry: Exploration, Environment, Analysis 4, 7–32.
Carranza, E.J.M., 2008. Geochemical Anomaly and Mineral Prospectivity Mapping in GIS. Elsevier, Amsterdam. 368 pp.
Carranza, E.J.M., 2011a. Analysis and mapping of geochemical anomalies using logratio-transformed stream sediment data with censored values. Journal of Geochemical Exploration 110, 167–185.
Carranza, E.J.M., 2011b. From predictive mapping of mineral prospectivity to quantitative estimation of number of undiscovered prospects. Resource Geology 61, 30–51.
Carranza, E.J.M., Owusu, E.A., Hale, M., 2009. Mapping of prospectivity and estimation of number of undiscovered prospects for lode gold, southwestern Ashanti Belt, Ghana. Mineralium Deposita 44, 915–938.
Chen, Y.Q., Liu, H.G., 2000. Delineation of potential mineral resources region based on geo-anomaly unit. Journal of China University of Geosciences 11, 158–163.
Chen, Y.J., Wang, Y., 2011. Fluid inclusion study of the Tangjiaping Mo deposit, Dabie Shan, Henan Province: implications for the nature of the porphyry systems of post-collisional tectonic settings. International Geology Reviews 53, 635–655.
Chen, Y.J., Pirajno, F., Qi, J.P., Li, J., Wang, H.H., 2006. Ore geology, fluid geochemistry and genesis of the Shanggong gold deposit, Eastern Qinling Orogen, China. Resource Geology 56, 99–116.
Chen, Y.J., Pirajno, F., Li, N., Guo, D.S., Lai, Y., 2009. Isotope systematics and fluid inclusion studies of the Qiyugou breccia pipe-hosted gold deposit, Qinling Orogen, Henan province, China: implications for ore genesis. Ore Geology Reviews 35, 245–261.
Clarke, D.S., Govett, G.J.S., 1990. Southwest Pacific epithermal gold: a rock-geochemistry perspective. Journal of Geochemical Exploration 35, 225–240.
Deng, J., Wang, Q.F., Wan, L., Yang, L.Q., Zhou, L., Zhao, J., 2008. Random difference of the trace element distribution in skarn and marbles from Shizishan ore field, Anhui Province, China. Journal of China University of Geosciences 19, 319–326.
Deng, J., Wang, Q.F., Yang, S.J., Liu, X.F., Zhang, Q.Z., Yang, L.Q., Yang, Y.H., 2009a. Self-similar fractal analysis of gold mineralization of Dayingezhuang disseminated-veinlet deposit in Jiaodong gold province, China. Journal of Geochemical Exploration 102, 95–102.
Deng, J., Yang, L.Q., Gao, B.F., Sun, Z.S., Guo, C.Y., Wang, Q.F., Wang, J.P., 2009b. Fluid evolution and metallogenic dynamics during tectonic regime transition: an example from the Jiapigou Gold belt in Northeast China. Resource Geology 59, 140–153.
Deng, J., Wang, Q.F., Yang, S.J., Liu, X.F., Zhang, Q.Z., Yang, L.Q., Yang, Y.H., 2010. Genetic relationship between the Emeishan plume and the bauxite deposits in Western Guangxi, China: constraints from U–Pb and Lu–Hf isotopes of the detrital zircons in bauxite ores. Journal of Asian Earth Sciences 37, 412–424.
Deng, J., Wang, Q.F., Wan, L., Liu, H., Yang, L.Q., Zhang, J., 2011a. A multifractal analysis of mineralization characteristics of the Dayingezhuang disseminated-veinlet gold deposit in the Jiaodong gold province of China. Ore Geology Reviews 53, 54–64.
Deng, J., Wang, Q.F., Xiao, C.H., Yang, L.Q., Liu, H., Gong, Q.J., Zhang, J., 2011b. Tectonic–magmatic–metallogenic system, Tongling ore cluster region, Anhui Province, China. International Geology Review 53, 449–476.
Deng, J., Yang, L.Q., Wang, C.M., 2011c. Research advance of superimposed orogenesis and metallogenesis in the Sanjiang Tethys. Acta Petrologica Sinica 27, 2501–2509 (in Chinese with English abstract).
Egozcue, J.J., Pawlowsky-Glahn, V., Mateu-Figueras, G., Barceló-Vidal, C., 2003. Isometric logratio transformations for compositional data analysis. Mathematical Geology 35, 279–300.
Eilu, P., Groves, D.I., 2001. Primary alteration and geochemical dispersion haloes of Archaean orogenic gold deposits in the Yilgarn Craton: the pre-weathering scenario. Geochemistry: Exploration, Environment, Analysis 1, 183–200.
Eilu, P., Mikucki, E.J., 1998. Alteration and primary geochemical dispersion associated with the Bulletin lode gold deposit, Wiluna, Western Australia. Journal of Geochemical Exploration 63, 73–103.
Fan, H.R., Xie, Y.H., Wang, Y.L., 1993. Magmatic hydrothermal characteristics of Huashani granite and its relationship with gold mineralization in Yuxi area. Acta Petrologica Sinica 9, 136–145 (in Chinese with English abstract).
Fedikow, M.A.F., Govett, G.J.S., 1985. Geochemical alteration haloes around the Mount Morgan gold–copper deposit, Queensland, Australia. Journal of Geochemical Exploration 24, 247–272.
Filzmoser, P., Hron, K., Reimann, C., 2009a. Univariate statistical analysis of environmental (compositional) data: problems and possibilities. Science of the Total Environment 407, 6100–6108.
Filzmoser, P., Hron, K., Reimann, C., Garrett, R., 2009b. Robust factor analysis for compositional data. Computers & Geosciences 35, 1854–1861.
Filzmoser, P., Hron, K., Reimann, C., 2012. Interpretation of multivariate outliers for compositional data. Computers & Geosciences 39, 77–85.
Ghavami-Riabi, R., Theart, H.F.J., De Jager, C., 2008. Detection of concealed Cu–Zn massive sulfide mineralization below eolian sand and a calcrete cover in the eastern part of the Namaqua Metamorphic Province, South Africa. Journal of Geochemical Exploration 97, 83–101.
Goldberg, I.S., Abranmson, G.Y.A., Los, V.L., 2003. Depletion and enrichment of primary haloes: their importance in the genesis of and exploration for mineral deposits. Geochemistry: Exploration, Environment, Analysis 3, 281–293.
Govett, G.J.S., Atherden, P.R., 1988. Applications of rock geochemistry to productive plutons and volcanic sequences. Journal of Geochemical Exploration 30, 223–242.
Govett, G.J.S., Dobos, V.J., Smith, S., 1984. Exploration rock geochemistry for gold, Parkes, New South Wales, Australia. Journal of Geochemical Exploration 21, 175–191.
Gray, J.E., Goldfarb, R.J., Detra, D.E., Slaughter, K.E., 1991. Geochemistry and exploration criteria for epithermal cinnabar and stibnite vein deposits in the Kuskokwim River region, southwestern Alaska. Journal of Geochemical Exploration 41, 363–386.
Gundobin, G.M., 1984. Peculiarities in the zoning of primary halos. Journal of Geochemical Exploration 21, 193–200.
Hacker, B.R., Wang, X., Eide, E.A., Ratschbacher, L., 1996. The Qinling–Dabie ultra-high-pressure collisional orogen. In: Yin, A., Harrison, M. (Eds.), The Tectonic Evolution of Asia. Cambridge University Press, Cambridge, pp. 345–370.
Han, Y.Y., Zhang, S.H., Pirajno, F., Zhang, Y.H., 2007. Evolution of the Mesozoic granites in the Xiong'ershan–Waifangshan region, western Henan Province, China, and its tectonic implications. Acta Geologica Sinica 2, 253–265.
Harraz, H.Z., 1995. Primary geochemical haloes, El Sid gold mine, Eastern Desert, Egypt. Journal of African Earth Sciences 20, 61–71.
Hawkes, H.E., Webb, J.S., 1962. Geochemistry in Mineral Exploration. Harper and Row, New York. 415 pp.
Howarth, R.J., Sinding-Larsen, R., 1983. Multivariate analyses. In: Howarth, R.J. (Ed.), Statistics and Data Analysis in Geochemical Prospecting. : Handbook of Exploration Geochemistry, Vol. 2. Elsevier, Amsterdam, pp. 207–289.
Hronsky, J.M.A., 2004. The science of exploration targeting. In: Muhling, J. (Ed.), SEG 2004, Predictive Mineral Discovery Under Cover. : Publication, 33. University of Western Australia, Centre for Global Metallogeny, pp. 129–133.
Hronsky, J.M.A., Groves, D.I., 2008. Science of targeting: definition, strategies, targeting and performance measurement. Australian Journal of Earth Sciences 55, 3–12.
Hu, S.X., Lin, Q.L., 1988. The Geology and Metallogeny of the Amalgamation Zone between Ancient North China Plate and South China Plate (Taking Qinling-Tongbai as an Example). Press of Nanjing University, Nanjing. 122 pp. (in Chinese).
Huston, D.L., 2001. Geochemical dispersion about the Western Tharsis Cu–Au deposit, Mt Lyell, Tasmania. Journal of Geochemical Exploration 72, 23–46.
Kaiser, H.F., 1960. The application of electronic computers to factor analysis. Educational and Psychological Measurement 20, 141–151.
Kitaev, N.A., 1991. Multidimensional analysis of geochemical fields. Mathematical Geology 23, 15–32.
Kroner, A., Compston, W., Zhang, G., Guo, A., Todt, W., 1988. Age and tectonic setting of Late Archean greenstone–gneiss terrain in Henan Province, China, as revealed by single-grain zircon dating. Geology 16, 211–215.
Large, R.R., McGoldrick, P.J., 1998. Lithogeochemical halos and geochemical vectors to stratiform sediment hosted Zn–Pb–Ag deposits, 1. Lady Loretta Deposit, Queensland. Journal of Geochemical Exploration 63, 37–56.
Levinson, A.A., 1974. Introduction to Exploration Geochemistry. Applied Publishing Ltd., Calgary. 611 pp.
Li, H.Q., Liu, J.Q., Wei, L., 1993. Geochronology and Geological Application of Fluid Inclusions in Hydrothermal Deposits. Geological Publishing House, Beijing. 126 pp. (in Chinese).
Li, H., Wang, Z.N., Li, F.G., 1995. Ideal models of superimposed primary halos in hydrothermal gold deposits. Journal of Geochemical Exploration 55, 329–336.
Li, H., Zhang, W.H., Chang, F.C., Zheng, T., Liu, B.L., Wang, Z.N., Tang, L., Liu, Z.C., Li, F.G., Wang, J.C., Guo, R.F., Geng, X.H., 1998. Primary Halo Model for Buried Ore Prospecting

of Large and Super-large Gold Deposits. Metallurgical Industry Press, Beijing. 125 pp. (in Chinese).
Li, H., Zhang, G.Y., Yu, B., 2006. Tectonic Primary Halo Model and the Prospecting Effect during Deep Buried Ore Prospecting in Gold Deposits. Geological Publishing House, Beijing. 146 pp. (in Chinese).
Lu, X.X., 1999. The Granites and the Tectonic Evolution of Qinling Orogenic Belt. Geological Publication House, Beijing. 35 pp. (in Chinese).
MacKenzie, D.J., Craw, D., Begbie, M., 2007. Mineralogy, geochemistry, and structural controls of a disseminated gold-bearing alteration halo around the schist-hosted Bullendale orogenic gold deposit, New Zealand. Journal of Geochemical Exploration 93, 160–176.
Mao, J.W., Xie, G.Q., Zhang, Z.H., Li, X.F., Wang, Y.T., Zhang, C.Q., Li, Y.F., 2005. Mesozoic large-scale metallogenic pulses in North China and corresponding geodynamic settings. Acta Petrology Sinica 21, 171–190 (in Chinese with English abstract).
McCuaig, T.C., Kerrich, R., 1998. P–T–t-deformation-fluid characteristics of lode gold deposits: evidence from alteration systematics. Ore Geology Reviews 12, 381–453.
McCuaig, T.C., Beresford, S., Hronsky, J., 2010. Translating the mineral systems approach into an effective exploration targeting system. Ore Geology Reviews 38, 128–138.
No.1 Geological Surveying Team, 1993. Study on the Geological Characteristics of Gold Deposits and Metallogenic Prediction in the Northern Xiong'er Mountains. Henan Bureau of Geology and Mineral Exploration and Development, Zhengzhou. 112 pp. (in Chinese).
No.1 Geological Surveying Team, 2003. Study on the Geochemical Characteristics and Metallogenic Prediction of Gold Deposits and Metallogenic Prediction of the Huanxiangwa Gold Deposit, Song County, Henan. Henan Bureau of Geology and Mineral Exploration and Development, Zhengzhou. 53 pp. (in Chinese).
Ovchinnikov, L.N., Grigorian, S.V., 1971. Primary halos in prospecting for sulphide deposits. Geochemical Exploration, CIM 11, 375–380.
Peres-Neto, P.R., Jackson, D.A., Somers, K.M., 2003. Giving meaningful interpretation to ordination axes: assessing loading significance in principal component analysis. Ecology 84, 2347–2363.
Pirajno, F., Bagas, L., 2008. A review of Australia's Proterozoic mineral systems and genetic models. Precambrian Research 166, 54–80.
Reimann, C., Filzmoser, P., 2000. Normal and lognormal data distribution in geochemistry: death of a myth. Consequences for the statistical treatment of geochemical and environmental data. Environmental Geology 39, 1001–1014.
Reimann, C., Garrett, R.G., 2005. Geochemical background—concept and reality. Science of the Total Environment 350, 12–27.
Reimann, C., Filzmoser, P., Garrett, R.G., 2002. Factor analysis applied to regional geochemical data: problems and possibilities. Applied Geochemistry 17, 185–206.
Reimann, C., Filzmoser, P., Garrett, R.G., 2005. Background and threshold: critical comparison of methods of determination. Science of the Total Environment 346, 1–16.
Reimann, C., Filzmoser, P., Garrett, R., Dutter, R., 2008. Statistical data Analysis Explained: Applied Environmental Statistics with R. John Wiley & Sons, Chichester. 362 pp.
Rose, A.W., Hawkes, H.E., Webb, J.S., 1979. Geochemistry in Mineral Exploration, 2nd edn. Academic Press, London. 637 pp.
Safronov, N.I., 1936. Dispersion haloes of ore deposits and their use in exploration. Problemy Sovetskoy Geologii 4, 41–53.
Schmid, S., Taylor, W.R., 2009. Significance of carbonaceous shales and vanadium geochemical haloes in the exploration for rock phosphate deposits in the southern Georgina Basin, central Australia. Journal of Geochemical Exploration 101, 91–92.
Sima, X.Z., 1997. An approach to the metallogenic mechanism of the ore-forming concentrated province of gold deposits in Huashan–Xiongershan Massif. Henan Geology 15, 167–174 (in Chinese).
Solovov, A.P., 1985. Geochemical Methods of Exploration for Mineral Deposits. Nedra, Moscow. 266 pp. (in Russian).
Sun, D.Z., Li, H.M., Lin, Y.X., Zhou, H.F., Zhao, F.Q., Tang, M., 1991. Precambrian geochronology, chronotectonic framework and model of chronocrustal structure of the Zhongtiao mountains. Acta Geology Sinica 65, 216–231 (in Chinese with English abstract).
Wang, C.M., Deng, J., Zhang, S.T., 2006a. Relationship between Huashan granite and gold mineralization in Xiongershan area, Henan. Geoscience 20, 315–321 (in Chinese with English abstract).
Wang, C.M., Deng, J., Zhang, S.T., Huang, S.M., Li, K.H., 2006b. Ore-forming fluid characteristics of Huanxiangwa deposit, Henan. Gold 27, 7–11 (in Chinese with English abstract).
Wang, C.M., Deng, J., Zhang, S.T., Huang, S.M., Li, K.H., 2006c. Relationship between wall-rock alteration and gold mineralization of Huanxiangwa deposit, Henan. Gold 27, 9–14 (in Chinese with English abstract).
Wang, C.M., Deng, J., Zhang, S.T., Huang, S.M., Li, K.H., 2007. Characteristic of primary halo and prediction of deep orebody of Huanxiangwa gold deposit, Henan. Geology and Prospecting 43, 58–63 (in Chinese with English abstract).
Wang, C.M., Cheng, Q.M., Deng, J., Xie, S.Y., 2008. Magmatic hydrothermal superlarge metallogenic systems—a case study of the Nannihu Ore Field. Journal of China University of Geosciences 19, 391–403.
Wang, C.M., Deng, J., Zhang, S.T., Xue, C.J., Yang, L.Q., Wang, Q.F., Sun, X., 2010a. Sediment-hosted Pb–Zn deposits in Southwest Sanjiang Tethys and Kangdian area on the western margin of Yangtze Craton. Acta Geologica Sinica 84, 1428–1438.
Wang, C.M., Deng, J., Zhang, S.T., Yang, L.Q., 2010b. Metallogenic province and large scale mineralization of VMS deposits in China. Resource Geology 60, 404–413.
Wang, Q.F., Deng, J., Liu, H., Wan, L., Zhang, R.Z., 2010c. Fractal models for ore reserve estimation. Ore Geology Reviews 37, 2–14.
White, D.E., 1981. Active geothermal systems and hydrothermal ore deposits. Economy Geology, 75th Anniversary Volume, pp. 392–423.
Yan, Z., 1993. Granites in Shaanxi Province. Press of Xi'an University of Transportation, Xi'an, pp. 1–110 (in Chinese).
Zhao, T.P., Zhuang, J.M., Yuan, Z.L., 1996. Rock types and volcanic series of Xiong'er Group on the southern margin of the North China Plate. Journal Geology and Mineral Research North China 11, 599–606 (in Chinese with English abstract).
Zhou, T.H., Lu, G.X., 2000. Tectonics, granitoids and Mesozoic gold deposits in East Shandong, China. Ore Geology Reviews 16, 71–90.